BATHYMETRIC, SEDIMENTOLOGICAL AND RETROSPECTIVE WATER QUALITY ANALYSIS TO EVALUATE EFFECTIVENESS OF THE LAKE ELSINORE RECYCLED WATER PIPELINE PROJECT

Final Report

Submitted to:

Lake Elsinore & San Jacinto Watersheds Authority
Riverside, CA 92503

Submitted by:

Michael Anderson
Dept. of Environmental Sciences
University of California – Riverside

15 September 2010

Table of Contents

List of Figures

List of Tables

Executive Summary

Lake Elsinore is the largest natural lake in Southern California. The lake is located at the base of San Jacinto River watershed, with hot dry summers and cool winters with highly variable annual precipitation. As a result of frequent drought and occasional El Nino conditions, the lake has varied widely in surface elevation, salinity and water quality. To reduce this variability, a number of management actions have been implemented. The Lake Elsinore Management Plan (LEMP) completed in 1995 substantially reconfigured the lake basin, reducing the lake area from about 6,000 acres to 3,000 acres, increasing lake mean depth and decreasing annual evaporative loss. Additional sources of water for the lake have also been developed to help stabilize lake levels and improve overall lake condition. Recycled water has been added to the lake, when levels drop below 1240', since 2002, making it the first natural lake in California to receive such inputs. More recently, mechanical surface mixers (2005) and a diffused aeration system (2008) have also been installed at the lake to enhance mixing and reduce the frequency and severity of fish kills, algal blooms and other problems that have plagued the lake. The recently completed Recycled Water Pipeline Project further enhances the capacity to deliver recycled water to the lake and help maintain lake level.

The purpose of this study was to better understand the influence of recycled water addition and related restoration measures on water quality and other conditions in Lake Elsinore. The study included: (i) characterization of sediment properties, comparing properties at 28 sites previously evaluated in 2000-2001; (ii) a detailed bathymetric and hydroacoustic survey of sediment properties and their distribution within the basin; and (iii) a retrospective review and statistical analysis of water quality data collected from 2000-2009.

A wide range of sediment properties were evaluated, including the concentrations of organic C , $CaCO_3$, total N, total P, inorganic and organic P, and porewater NH_4-N and PO_4-P concentrations. Grouping the different sediments into the 3 types proposed in Anderson (2001) yielded no statistically significant differences for properties except for increased $CaCO_3$ in the fine organic (type III) sediments in 2010 relative to concentrations measured in 2000. Non-parametric statistical tests over the entire dataset (i.e., without prior assumptions about clustering of data) indicated that the sediments in 2010 had a slightly higher sand content, and increased porewater PO_4-P concentrations, but somewhat lower organic C concentration, loss-on-ignition, and

porewater NH_4-N. Overall, current sediment properties do not provide clear evidence of changes in sediment quality over the past decade. That is, recycled water additions and related management actions implemented over the past decade have not substantively improved nor degraded sediment quality based upon these measurements.

Nutrient flux and sediment oxygen demand (SOD) rates were measured at 3 sites, representing the type I, II and III sediments, in August for direct comparison with measurements made in August 2001 (Anderson, 2001). The mean flux of PO_4-P from the fine organic type III sediment at low native DO concentrations (0.5 mg L^{-1}) increased from 10.1±0.3 in 2001 to 12.8±1.2 mg m^{-2} d^{-1} in 2010, while flux from the type II sediment decreased from 10.5±0.9 to 7.8±3.1 mg m^{-2} d^{-1}. The coarse-textured type I sediment was found to release PO_4-P at a slow rate in 2001 (1.9±0.9 mg m^{-2} d^{-1}), while it took up PO_4-P at a slow rate (-1.1±0.2 mg m^{-2} d^{-1}) from the water column in 2010. Mean NH_4-N flux was somewhat higher in 2010 in the type I and III sediments and unchanged in the type II sediments. Aeration was found to reduce PO_4-P flux by 29% in the fine organic type III sediments, but had less of an effect on the other sediments. Average NH_4-N flux rates were not significantly altered as a result of aeration.

Additional measurements provided new information about sediment biogeochemistry. *In situ* measurements of gas volume found negligible volumes in March, but very high volumes of gas were present within the sediments in July and August. The volumes of gas within sediments in the summer were generally 1-2 L m^{-2} at most sites, with a maximum measured volume of almost 6 L m^{-2} in a silt-rich sediment near the mouth of the channel leading to the San Jacinto River input to the lake. The gas there was elevated in CO_2 over 100x that found in air (3.8±0.6% CO_2 by volume, compared with approximately 0.035% in air), reflecting rapid rates of microbial respiration and decomposition in the warm summer sediments. No significant O_2 was measured in the gas samples, with most of the remaining gas as N_2.

Microprofile measurements of pH and redox indicate limited penetration of DO into the sediment under vigorous aeration; aeration at a rate that is estimated to be over 1000x more rapid that the lake-wide average aeration rate achieved DO penetration 3-4 mm after 1 week. This clearly reflects the intense microbial activity occurring near the surface of the sediments. Sequential extraction of surface sediments demonstrate significant quantities of reactive iron-sulfide minerals present, with FeS(am) and Fe_3S_4 in sufficient quantities to exert a significant demand for oxygen. The quantities of extractable reduced Fe(II)-sulfide and oxidized Fe(III) minerals exhibited no significant

difference in a transect between two adjacent diffuser lines, implying the diffused aeration system has not been able to favorably alter sediment biogeochemical conditions there. Observations about sediment color support this conclusion.

In addition to these direct, detailed sedimentological measurements, multi-frequency hydroacoustics were used to determine depth to sediments and sediment acoustical properties. Surveys on transects totaling 270 km in length were conducted over 6 days in late June and early July. All hydroacoustic data were georeferenced using realtime differential GPS that allowed development of detailed bathymetric maps and maps of acoustically-inferred sediment properties based upon the strong correlation between the fractal dimension of the bottom echo and organic C content, % water content and other sediment properties.

Finally, water quality data from 2000-2009 were reviewed and statistically analyzed. The mean summer chlorophyll a concentrations over the past 10 years were found to be significantly correlated with maximum depth, and concentrations of total N and TDS (r^2 = 0.58, 0.62 and 0.49, respectively, but not correlated with total P or total N: total P ratios (r^2 = 0.02 and 0.10, respectively). Lake level and TDS thus appear to be more important predictors of summer chlorophyll a concentrations that total P concentrations in the lake.

1. INTRODUCTION

Lake Elsinore is the largest natural freshwater lake in Southern California, with a nominal surface area of approximately 3000 acres. The lake is located at the base of the 760 mi^2 (2000 km^2) San Jacinto River watershed in a down-faulted trough and bordered to the west by the Santa Ana Mountains that form the northernmost range of the Peninsular Ranges Province (FERC, 2006).

The Mediterranean climate in the region results in hot dry summers with annual evaporation exceeding 1.4 m yr^{-1}. The El Nino-drought cycle often results in several consecutive years of limited rainfall and low runoff, leading to rapid reductions in lake level and increased salinity, followed by extensive runoff and potential for flooding under extreme conditions. To help reduce the severity of the flood-drought cycle, the surface area of the lake was reduced from approximately 6,000 acres to 3,000 acres as part of the US. Bureau of Reclamation-sponsored Lake Elsinore Management Plan that was completed in 1995. Following this, additional sources of water were also developed to help stabilize lake level, including local groundwater and recycled water, making it the first natural lake in California to receive recycled water inputs. Recycled water has been added since 2002 when the lake surface elevation has dropped below 1240' above MSL. The Recycled Water Pipeline Project, supported by the SWRCB, expanded the capacity to deliver recycled water to the lake.

The purpose of this study is to better understand the effects and effectiveness of adding recycled water to improve overall conditions and water quality in the lake. This study includes: (i) characterization of sediment properties, comparing properties at 28 sites previously evaluated in 2000-2001; (ii) a detailed bathymetric and hydroacoustic survey of sediment properties and their distribution within the basin; and (iii) a retrospective review and statistical analysis of water quality data collected from 2000-2009.

2. SEDIMENT CHARACTERIZATION

2.1 Sediment Physical and Chemical Properties

2.1.1 Methods

Sediment grab samples were collected from 28 of the 49 sites on the lake that were previously sampled (Anderson, 2001) (Fig. 2.1).

Fig. 2.1 Locations of sediment grab samples collected in May 2010.

Grab samples were collected in May 2010 and analyzed for the same properties as in the prior study (Anderson, 2001), as well as some new measurements (Table 2.1).

Table 2.1. Sediment properties, characterization and measurements.		
Sediment		**Porewater**
Physical	*Chemical*	*Chemical*
% Water Content	% Organic C	NO_3-N
Particle Size	% $CaCO_3$	NH_4-N
Loss on Ignition	Total N	PO_4-P
Munsell Color	Total P	Fe^{2+}
	Inorganic P	Mn^{2+}
	Organic P	pH
	Reductant-soluble P	
	Fe speciation	

Sediment samples were collected using an Ekman dredge that sampled the uppermost ~10 cm of sediment; the sediments were then briefly homogenized by mixing with a plastic spoon, and approximately 600 g wet weight sediment were then transferred to 500 mL glass wide-mouthed jars. The jars were filled to the top with no headspace, capped with Teflon-lined lids and placed on ice for transport back to the laboratory.

Sediment was promptly homogenized and subsampled for sediment characterization and porewater analysis. Water content was determined on subsamples that were heated overnight at 105 °C. This higher temperature, commonly used in soil analyses, was chosen over the lower temperatures (60-80 °C) used by Hakanson and Jansson (1983) and others because of the high amount of hydrous clays and moderate organic matter content found in these sediments. Particle size was determined on samples mechanically dispersed in sodium hexametaphosphate without $CaCO_3$ or organic matter removal using the hydrometer method (Gee & Bauder, 1986). Total C, N, and S were measured by dry-combustion methods using a Thermo Flash EA NC soil analyzer (Nelson & Sommers, 1982). Inorganic C and $CaCO_3$ were determined manometrically following Loeppert & Suarez (1996). Organic C was taken as the difference between total C and inorganic C. Total and inorganic P was determined following Aspila et al. (1976). Organic P was taken as the difference between total and inorganic P (Aspila et al., 1976; Berner & Rao, 1994). Porewater was extracted by centrifugation, filtered through 0.45 μm polycarbonate filters fitted to disposable plastic syringes, and acidified with reagent-grade H_2SO_4. Porewater NH_4-N and dissolved orthophosphate (PO_4-P) and extracted P were analyzed using a Technicon autoanalyzer following standard methods (APHA, 1998). Porewater Fe^{2+} and Mn^{2+} concentrations on separate filtered porewater samples acidified with metals-grade HNO_3 were determined using a Perkin-Elmer 3000DV ICP-OES.

Sediment color was quantitatively evaluated using the Munsell color system developed for soils, including hydric/wetland soils. Soil colors that are grey to bluish-green represent soils with significant quantities of Fe^{2+} present, as found in poorly drained soils and anaerobic conditions, while yellow, brown to reddish colors indicate the presence of Fe in the oxidized (Fe^{3+}) form typical of well-aerated soils. Sheets from the Munsell soil color book representing gleyed colors associated with saturated, anaerobic soils, and colors commonly found in well-aerated soils are shown in Fig. 2.2.

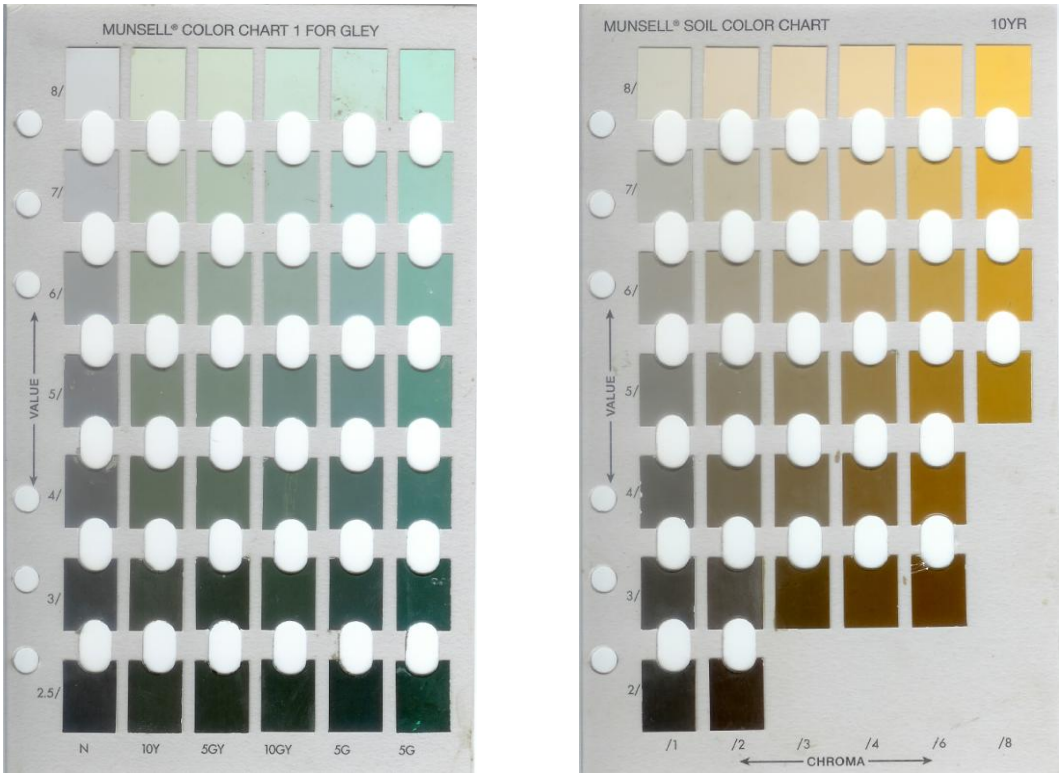

Fig. 2.2. Example sheets from Munsell Soil Color Book: a) Gley1 and b) 10YR.

2.1.2 Results

Cluster analysis of properties of sediment samples collected in 2000 led to classification of bottom sediments into 3 types that varied in their texture, organic C content, nutrient concentrations and other properties (Anderson, 2001). Resampling of 28 of the original 49 sites allows us to compare in an average way how sediment properties may have changed over the past 10 years (Table 2.2).

Retaining the original type classification, the coarse-textured, low organic C sediment (type 1) was found to have slightly lower mean sand contents and increased silt and clay, although the variance was very large. Mean organic C, $CaCO_3$, total N and P contents also increased although changes were not statistically significant based upon standard parametric tests owing to the large variance and modest n size (n= 8) within the type I sediments.

Table 2.2. Mean sediment properties comparing results with 2000 (Anderson, 2001).							
MEAN PROPERTY	**Units**	**Type I**		**Type II**		**Type III**	
		2000	**2010**	**2000**	**2010**	**2000**	**2010**
Sand	%	70.8 ± 31.2	62.3±32.7	29.5 ± 15.4	44.9±37.7	4.1 ± 4.0	1.7±2.1
Silt	%	19.7 ± 23.6	25.0±15.8	48.1 ± 11.9	41.9±29.9	44.8 ± 6.8	46.0±11.4
Clay	%	9.5 ± 11.7	11.8±19.1	22.3 ± 5.4	13.2±7.9	51.2 ± 6.3	52.3±11.1
Total C	%	1.07 ± 1.44	1.42±2.52	3.04 ± 0.86	2.4±1.8	5.97 ± 0.39	6.29±0.43
Organic C	%	0.79 ± 1.06	0.96±1.77	2.13 ± 0.75	1.4±1.2	4.84 ± 0.45	4.38±0.43
Inorganic C	%	0.28 ± 0.42	0.46±0.78	0.90 ± 0.20	1.0±0.8	1.14 ± 0.26	1.91±0.15
$CaCO_3$	%	2.34 ± 3.46	3.85±6.52	7.53 ± 1.66	8.7±6.7	9.5 ± 2.2[a]	15.95±1.24
Total N	%	0.10 ± 0.12	0.14±0.22	0.27 ± 0.07	0.30±0.06	0.53 ± 0.03	0.52±0.04
Total P	mg/kg	425 ± 209	756±393	781 ± 165	842±393	916 ± 73	785±588
Inorganic P	mg/kg	340 ± 170	558±355	595 ± 128	685±284	573 ± 77	594±340
Organic P	mg/kg	84 ± 97	197±308	196 ± 104	156±120	342 ± 71	191±297
SRP	mg/L	0.6 ± 1.3	1.8±3.3	3.1 ± 0.6	4.5±0.6	4.9 ± 1.2	5.7±0.9
NH_4-N	mg/L	6.8 ± 6.9	4.9±3.7	14.5 ± 6.1	12.7±3.9	20.0 ± 3.7	16.3±2.5

The type II sediments varied somewhat less over time and generally not in a statistically significant way (Table 2.2). The content of $CaCO_3$ was found to be significantly increased in the type III sediments ($p=0.001$), although other changes were not significant. For example, the average total N content within the fine-textured type III sediments was unchanged (0.53±0.03 % in 2000 vs. 0.52±0.04 % in 2010) (Table 2.2). The mean total P concentration varied somewhat more (916±73 and 785±588 mg kg^{-1}, respectively), although the large variance in 2010 yields no statistically significant difference in the values. The amounts as inorganic P were very similar in 2000 and 2010, with no significant difference in organic P in place either (Table 2.2). The increase in $CaCO_3$ concentration in the deeper, finer textured (type III) sediments is thought to have resulted from increased precipitation of $CaCO_3$ within the water column and sediments due to the high salinities, high algal productivity and elevated pH values in 2003-2004, in combination with erosion and deposition of calcareous soils into the lake basin during the El Nino event of 2005.

Non-parametric statistical tests (sign tests) were also used to explore possible changes in sediment properties. Non-parametric tests are appropriate for non-normally distributed data, especially where paired data sets are available. Such an analysis on the entire data set revealed somewhat different conclusions (Fig. 2.3).

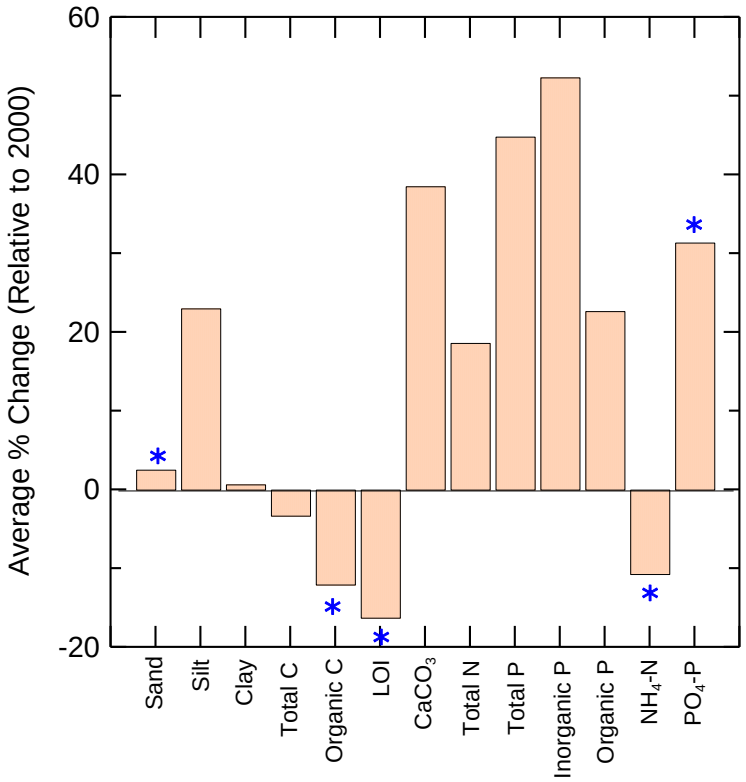

Fig. 2.3. Average % change in sediment properties using non-parametric sign test.

Based upon non-parametric sign tests over the entire dataset (*i.e.*, without prior assumptions about clustering of data), a number of properties were found to be significantly different (at $p<0.05$) between the 2 sampling events (designated by the *) (Fig. 2.3). The fraction of sand was found to be slightly but statistically significantly increased, on average, relative to 2000, while PO_4-P concentrations in sediment porewater were more significantly increased, by about 30% relative to 2000. While other properties also increased on average, the changes were not statistically significant. Modest but statistically significant average reductions in organic C concentration (about 11% reduction), loss on ignition (LOI, correlated with organic C concentration), and reductions in porewater NH_4-N concentrations were also found (Table 2.2).

The apparent reduction in organic C and increase in average sand content in the bottom sediments probably reflect increased inputs and deposition of inorganic soils eroded off the watershed and deposited into the lake basin, effectively diluting autochthonously derived organic C (Rowan et al., 1992). Given the strong seasonal differences in porewater nutrient concentrations in the lake (Anderson, 2001), caution is

warranted in interpretation of the changes in dissolved NH_4-N and PO_4-P concentrations in the sediment porewater.

In general, sediment properties do not provide clear evidence of changes in sediment quality over the past decade. These properties do, nonetheless, (i) provide insights into the biogeochemical conditions of the sediments, and (ii) serve to ground-truth hydroacoustic data, potentially allowing for basin-wide representations of critical sediment characteristics such as rates of internal nutrient recycling and sediment oxygen demand (SOD).

As a first step toward understanding the biogeochemical conditions of the bottom sediments and the relationships that exists between different physical and chemical properties, a correlation matrix was developed (Table 2.3). At an n size of 28, an r-value >0.478 is statistically significant at p=0.01, although statistical significance does not necessarily imply significance in terms of sediment quality. The square of r is arguably more useful, since it defines the fraction of the variance in the response variable accounted by the explanatory variable. Thus, for example, with an r of 0.55 (significant at p=0.01), only 30% of the variance in porewater PO_4-P is accounted for by sediment depth. In contrast, 76% of the variance in porewater PO_4-P concentrations in the lake sediments can be accounted for by sediment organic C concentrations (r=0.87) (Table 2.3). We see that organic C content, as well as total C, are highly correlated with other relevant sediment properties, including total N, porewater NH_4-N and clay concentrations.

Table 2.3. Correlation matrix for measured sediment properties. An r-value >0.478 is statistically significant at p=0.01.

Property	Depth	Sand	Silt	Clay	% H_2O	GasVol	Total C	Org C	L.O.I.	Inorg C	$CaCO_3$	Total N	Total P	Inorg P	Orgc P	NH_4-N	PO_4-P
Depth	1																
Sand	-0.79	1															
Silt	0.54	-0.82	1														
Clay	0.77	-0.87	0.43	1													
% H_2O	0.83	-0.98	0.76	0.89	1												
Gas Vol	0.36	-0.67	0.82	0.36	0.63	1											
Total C	0.84	-0.97	0.69	0.93	0.98	0.57	1										
Org C	0.82	-0.95	0.66	0.93	0.96	0.51	0.99	1									
L.O.I.	0.85	-0.96	0.67	0.93	0.97	0.51	0.99	0.98	1								
Inorg C	0.82	-0.93	0.72	0.84	0.96	0.66	0.94	0.89	0.92	1							
$CaCO_3$	0.82	-0.93	0.72	0.84	0.96	0.66	0.94	0.89	0.92	1.00	1						
Total N	0.72	-0.84	0.55	0.85	0.87	0.47	0.90	0.90	0.90	0.83	0.83	1					
Total P	0.02	-0.24	0.11	0.29	0.27	0.24	0.22	0.22	0.15	0.19	0.19	0.18	1				
Inorg P	0.00	-0.27	0.18	0.27	0.30	0.34	0.23	0.22	0.18	0.22	0.22	0.25	0.82	1			
Org P	0.10	-0.15	-0.02	0.25	0.16	0.01	0.16	0.17	0.12	0.14	0.14	0.05	0.68	0.16	1		
NH_4-N	0.60	-0.89	0.49	0.75	0.92	0.49	0.92	0.88	0.88	0.88	0.88	0.86	-0.04	-0.03	-0.03	1	
PO_4-P	0.55	-0.87	0.35	0.82	0.90	0.46	0.90	0.87	0.84	0.85	0.85	0.84	0.21	0.19	0.14	0.92	1

2.2 Nutrient Flux and Sediment Oxygen Demand

2.2.1 Methods

In addition to the characterization of sediment samples, intact sediment cores were collected on August 9 from 3 sites to quantify sediment oxygen demand (SOD) and sediment nutrient flux rates under ambient conditions and with aeration as in previous studies (Anderson, 2001; Anderson, 2007). Two sets of triplicate cores were collected from sites reflecting the 3 sediment types previously identified in the lake (Anderson 2001) (Table 2.4). Sediment surface color at the time of sampling was recorded.

Table 2.4. Location and basic characteristics of core samples.

Site	Type	Latitude	Longitude	Depth (m)	% H_2O	% OrganicC
SW	I	33.6599	-117.3699	3.5	21.9	<0.1
L	II	33.6710	-117.3649	6.3	69.5	3.43
HSZ	III	33.6657	-117.3523	7.2	82.3	4.35

Briefly, an Ekman dredge was used to collect a grab sample, which was then subsampled by carefully inserting a 30.5 cm by 6.3 cm diameter Lucite tube approximately 10 cm into the sediment. The bottom of the core was sealed using a rubber stopper and secured. The core was then carefully topped off with bottom water sampled using a van Dorn sampler and stoppered with zero headspace. Cores

One set of cores from each site were then incubated in the dark at 26°C under aeration while the second set was incubated at the DO levels measured at the time of sampling. Approximately 10 mL of water was removed daily for 7 days, filtered and analyzed for soluble NH_4-N, NO_3-N and SRP using the Technicon autoanalyzer following standard methods (APHA, 1989). Dissolved oxygen was measured using a YSI Model 55 DO meter. The water was briefly sparged with N_2 or lab air as needed to maintain DO and to very gently mix the water column within core maintained near lake conditions. Care was taken to not disturb the sediment when sampling or sparging. The measured change in concentration was used in conjunction with water volume and sediment-water interfacial area to calculate a mass flux rate. Sediment color for the cores maintained near ambient (low) DO levels and those that were aerated were also recorded.

Following completion of the nutrient flux measurements, sediment oxygen demand (SOD) was measured on the set of aerated cores. Initial DO concentrations and DO concentrations over time were recorded for sealed cores. Separate

measurements of water oxygen demand (WOD) were also made. SOD was calculated from the measured loss in DO over time, the volume of overlying water, and the cross-sectional/surface area of the cores after correction for WOD.

2.2.2. Results

Ammonium-N and PO_4-P concentrations increased approximately linearly with time reflecting release from sediments and accumulation in the overlying water (e.g., Fig. 2.4). Some variability between triplicate cores were observed; in this example, one core released less NH_4-N and substantially less PO_4-P than the other two cores (Fig. 2.4, open circles).

Observed changes in concentration over time were converted to flux estimates based upon known volume of overlying water and sediment surface area (Table 2.5). Included in this table are results from measurements made in August 2001. As previously noted, NH_4-N and PO_4-P are released at significant rates from the finer-textured sediments in the lake (e.g., HSZ and L sites), while much lower release was found in the shallow, coarse-textured sediment (Table 2.5). Nutrient flux rates at these 3 sites were generally similar to rates found in 2001, with lower rates of PO_4-P release from the SW and L sites, but increased flux rates at the HSZ site (Table 2.5). Measured NH_4-N flux rates were similar (L site) or somewhat higher (SW and HSZ sites) in 2010 when compared with flux rates found in 2001.

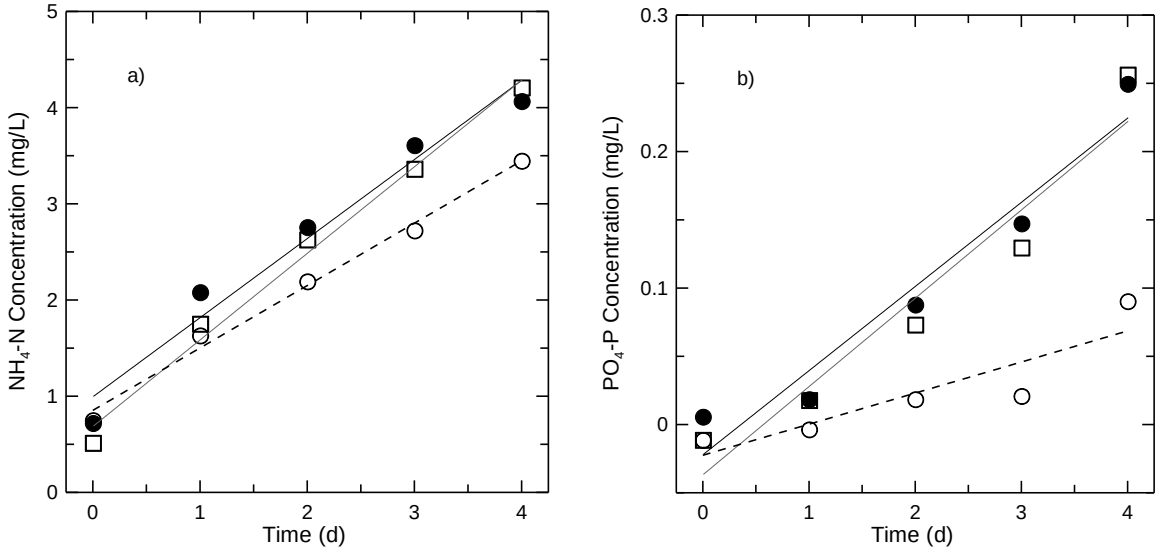

Fig. 2.4. Example of core-flux results for limnocosm site at DO concentration similar to that present in field (1.5-2 mg L^{-1}):. a) NH_4-N and b) PO_4-P.

Table 2.5. Nutrient flux rates comparing results with 2000-2001 (Anderson, 2001).							
Site	**Type**	**DO ($mg\ L^{-1}$)**		**PO4-P Flux ($mg\ m^{-2}\ d^{-1}$)**		**NH4-N Flux ($mg\ m^{-2}\ d^{-1}$)**	
		2001	**2001**	**2001**	**2010**	**2001**	**2010**
SW	I	3.5	1.4	1.9±0.9	-1.1±0.2	10.1±4.6	30.1±2.0
L	II	2.0	1.5	10.5±0.9	7.8±3.1	122±19.1	123.9±7.8
HSZ	III	0.6	0.5	10.1±0.3	12.8±1.2	101.0±15.9	128.5±9.0

Aeration was found to reduce the rates of PO_4-P and NH_4-N flux from bottom sediments when compared to rates measured under typical summer DO concentrations (Table 2.6). The reduction in mean PO_4-P flux for the type III sediments was 29%, broadly similar to reductions found in other studies for Lake Elsinore and Canyon Lake, although aeration lowered PO_4-P flux only 8% in the type II sediment sampled here.

Table 2.6. Effect of aeration on nutrient flux rates.							
Site	**Type**	**DO ($mg\ L^{-1}$)**		**PO4-P Flux ($mg\ m^{-2}\ d^{-1}$)**		**NH4-N Flux ($mg\ m^{-2}\ d^{-1}$)**	
		2010	**2010+Air**	**2010**	**2010+Air**	**2010**	**2010+Air**
SW	I	1.4	5.2	-1.1±0.2	-1.1±0.2	30.1±2.0	8.7±15.6
L	II	1.5	5.5	7.8±3.1	7.2±2.1	123.9±7.8	121.9±28.9
HSZ	III	0.5	6.3	12.8±1.2	9.1±1.1	128.5±9.0	119.6±26.9

Although a full characterization of the properties of these sediments was not conducted, % water content was measured (82.3, 69.5 and 21.9% for HSZ, L and SW sediment, respectively). As noted in Table 2.3, % water content is very highly correlated with % organic C content and porewater NH_4-N and PO_4-P (r=0.96, 0.92 and 0.90, respectively). From a linear regression of the data from the 28 sites, we predict the % organic C in these 3 sediments at 4.4, 3.4 and <0.1% % (Table 2.4). Although the n-size is low (n=3), a trend is seen relating NH_4-N and PO_4-P flux to organic C content (and porewater NH_4-N, PO_4-P and % water content) (Fig. 2.5).

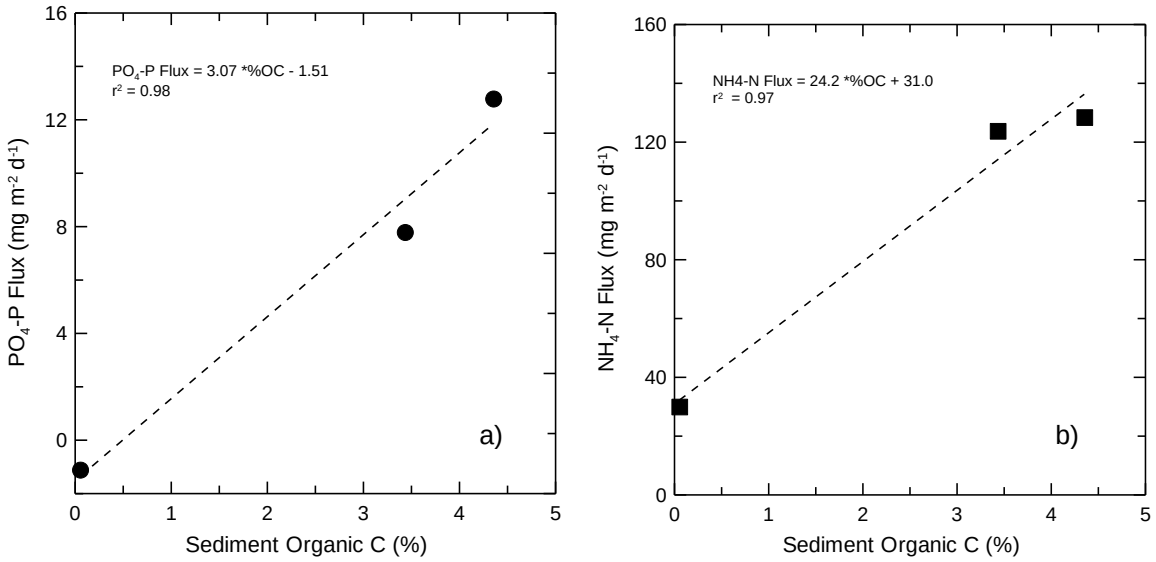

Fig. 2.5. Nutrient flux rates vs. organic C content: a) PO_4-P flux and b) NH_4-N flux.

Following the end of the nutrient flux measurements, the aerated cores were then topped off with lake water to establish zero-headspace, briefly sparged with air, and initial DO concentrations measured. Following this, the cores were capped, maintained at 26.0±0.5 ºC in the dark, and DO levels were measured after 23 and 48 h to determine the rate of sediment oxygen demand. Water oxygen demand was measured by monitoring DO concentrations in separate water samples stored in brown polypropylene bottles at the same temperature. Loss of DO in overlying water in the cores was corrected for WOD to determine SOD values for these 3 replicate sampling sites (Table 2.7). Water oxygen demand at the time of these measurements was very high (1.65±0.23 mg L^{-1} d^{-1}), a value over 50% higher than found in earlier measurements for Lake Elsinore and Canyon Lake (which have been typically closer to 1 mg L^{-1} d^{-1}). This is presumably due to the high algal levels and low transparencies present in the lake at time of sampling (Z_{sd} of 0.3 - 0.4 m). SOD values increased from 0.27±0.03 g m^{-2} d^{-1} for the sandy, low organic C sediments, to 0.62±0.26 g m^{-2} d^{-1} for the type II sediments, and 0.93±0.03 g m^{-2} d^{-1} for the high organic C type III sediments (Table 2.7). SOD was strongly correlated (r^2=0.92) with % organic C (%OC) (as predicted from % water content) by the equation:

$$SOD\ (g\ m^{-2}\ d^{-1}) = 0.14\ \%OC + 0.24 \qquad (2.1)$$

Table 2.7. Rates of summer sediment oxygen demand (SOD).		
Site	**Type**	**SOD ($g\ m^{-2}\ d^{-1}$)**
5-1	I	0.27±0.03
3-2	II	0.62±0.26
4-5	III	0.93±0.03

2.3 Sediment Gas Production and Ebullition

Gas production and composition within bottom sediments reflects the types of biogeochemical processes operating there (*e.g.*, respiration, denitrification, sulfate reduction). Moreover, ebullition can be an important transport process enhancing diffusive transport of nutrients from sediments to the overlying water column.

2.3.1 Methods

Measurements of the sediment gas volume per unit area ($L\ m^{-2}$) were made at 7 sites on the lake (Fig. 2.6). Gas samples were collected by briefly lowering a weighted stainless steel disk of known cross-sectional area (62 cm^2) onto the sediment, thereby displacing gas from the sediment, and capturing the gas bubbles into an inverted funnel that directs bubbles into a clear plastic measuring tube filled with water. The bubbles displace water from the measurement tube, and the volume of displaced water/released gas is measured at the water surface. Due to the compressibility of gas, the gas volume at the sediment depth was calculated from the gas volume measured at the lake surface, sediment depth, hydrostatic pressure and ideal gas law.

Gas samples were separately collected into 30 mL vials fastened to the funnel, brought to the surface, and sealed using a Teflon-lined cap fitted with a gas-sampling valve on August 7 from site G-3 (Fig. 2.6). Samples were returned to the lab and analyzed by direct gas injection into a Hewlett-Packard series 5890/5970 GC-MS using selective-ion monitoring.

Fig. 2..6. Sediment gas sampling sites (lines represent hydroacoustic transects across sites.)

2.3.2 Results

Gas volumes in the sediments were very low or below detection in the initial sampling conducted on March 15, 2010, reflecting the cool winter temperatures and low rates of microbial activity in the lake (Fig. 2.7a). Gas volumes increased markedly during the summer, with volumes generally 1-2 L m^{-2} at most of the sites, and approaching 6 L m^{-2} at site G-3 (near the entrance to the ski school , Fig. G-3). Sampling later in August revealed similar patterns across the 7 sites, although somewhat lower gas volumes were generally present (Fig. 2.7b,c).

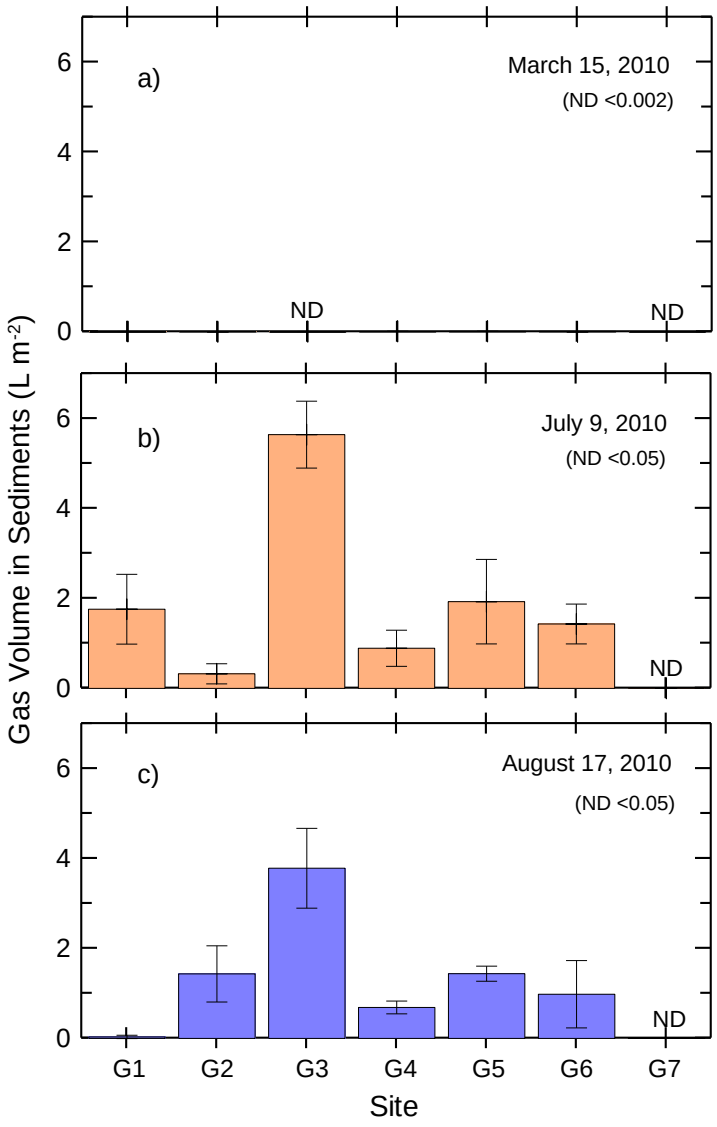

Fig. 2.7. Gas volume in sediments: a) March 15, b) July 9, and c) August 17, 2010.

Analysis of the gas samples by GC-MS revealed levels of CO_2 that were elevated over 100x that found in the atmosphere (3.8±0.6% CO_2 by volume, compared with approximately 0.035% in air). No significant O_2 was present in the gas samples, although most of the gas in the sediments was present as N_2. Methane analyses were not conducted, but sulfate reduction is known to inhibit methanogenesis, so H_2S is a more likely component of the sediment gas than methane.

Microbial respiration reactions have thus greatly increased local CO_2 concentrations in the sediments, resulting in supersaturation and formation of discrete gas bubbles into which N_2 dissolved in water partitions (the non-dimensional Henry's

constant for N_2 is 63.9 at 25°C, meaning that at equilibrium there is 63.9x more N_2 in the gas phase than dissolved in water). Respiration reactions producing CO_2 include aerobic processes as well as use by specialized microbes of other electron acceptors such as sulfate. The relative amount of C utilized by aerobic bacteria and anaerobic bacteria can be crudely estimated assuming that the DO concentration in the sediment porewater originally was near saturation (about 8 mg L^{-1}); if all of that DO was utilized by aerobic bacteria for mineralization of organic matter, somewhere around 11 mg L^{-1} CO_2 would be expected in the water and 13 mg L^{-1} in gas bubbles, since the non-dimensional Henry's constant for CO_2 is about 1.2 at 25ºC. The 3.8% CO_2 by volume measured in sediment gas is equivalent about 65 mg L^{-1} in the gas phase, so this suggests that only about 20% of the CO_2 present in the sediment gas bubbles could have been produced by aerobic processes. Use of other electron acceptors, thought to be principally sulfate, clearly drive organic matter decomposition in the sediments of Lake Elsinore.

Assuming the concentration of CO_2 in gas bubbles within the sediment is in local equilibrium with the water phase, one can predict the pH of the sediment porewater from:

$$pH = -\log\left(\frac{K_{a1}[CO_2(aq)]}{[HCO3^-]}\right) \qquad (2.2)$$

where K_{a1} is the first dissociation constant for carbonic acid (H_2CO_3) ($4x10^{-7}$ M), $[CO_2(aq)]$ is the molar aqueous concentration of CO_2 and $[HCO_3^-]$ is the molar concentration of bicarbonate dissolved in water. Based upon bicarbonate concentrations found in the sediment from previous peeper studies of about 15-25 mM (Anderson, 2001) and CO_2 aqueous phase concentrations based upon CO_2 concentrations in sediment gas samples assuming a non-dimensional Henry's constant of 1.2, one predicts sediment pH values of about 7.4. Microelectrode measurements that explore pH and redox potential near the sediment water interface are described below.

2.4 Microprofile pH and Redox Potential Measurements

2.4.1 Methods

Fine scale vertical profiles of pH and redox potential were measured using Microelectrode Inc. capillary pH and redox microelectrodes with 1.3 mm outer tip diameters fastened to a Lory type-A micrometer with 0.3 mm vertical precision. The

electrodes were connected to a dual channel AccuMet AR-25 pH meter via BNC connectors and calibrated prior to measurements.

Six intact cores from the HSZ site were collected on August 18 and returned to the lab, where two cores were vigorously aerated for 1 week at a rate of ~200 cm^3 min^{-1} (for an aeration rate, normalized to the sediment surface area, of about 6.5 cm^3 cm^{-2} min^{-1}). This rate is estimated to be >1000x larger than that for the diffused aeration system installed at the lake. A second pair of cores were not aerated and allowed to go anoxic, as would be the case when high SOD and WOD is in place, and stratification limits natural mixing. The final two cores were put aside and not used in these measurements.

2.4.2 Results

Microprofile measurements reveal strong pH and redox potential gradients exist near the sediment-water interface (Fig. 2.8). The aerated cores exhibited relatively high pH conditions (pH near 8.6) and large positive redox potentials in the water above the sediments (Fig. 2.8a). Measured pH and redox potentials both declined sharply across the sediment-water interface, with a reduction from almost +200 mV in the overlying water to –160 mV about 4 mm below the interface (Fig. 2.8a). Large positive redox values indicate oxidizing conditions, with O_2 serving as the primary electron acceptor. Thus, aeration of the cores achieved favorable redox conditions in the overlying water (DO concentration was 7.4 mg L^{-1}), although penetration into the sediments was limited to the uppermost 3-4 mm. Despite very rapid aeration for an extended period of time (1 week), microbial and related biogeochemical processes limited the downward penetration of oxygen into the sediments. Large amounts of labile organic matter, such as algal detritus and zooplankton fecal pellets, help fuel extensive microbial decomposition reactions, resulting in high rates of SOD (section 2.2). Such rates exceed diffusion rates for O_2 into the sediments and results in the sharp redox potential gradients observed. The large negative redox potential found a short distance into the sediments is indicative of strongly reducing conditions. Values of –160 mV are consistent with sulfate reduction, which typically occurs at redox values of –100 to –200 mV (Wetzel, 2001).

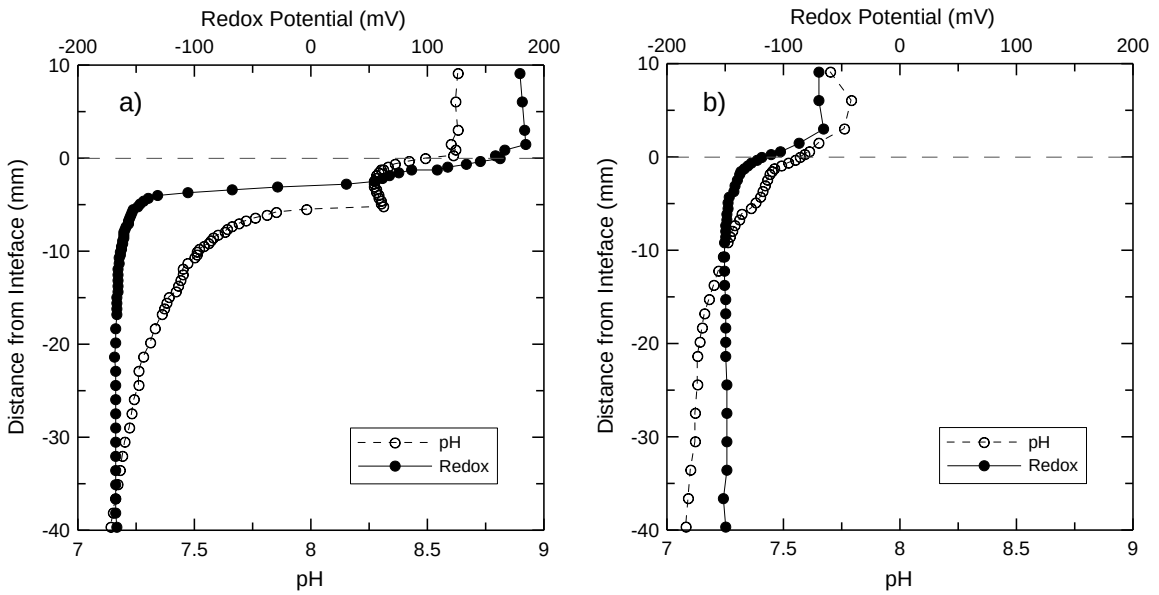

Fig. 2.8. Microelectrode profile measurements: a) aerated core (DO = 7.4 mg L-1) and b) anoxic core (DO = 0.2 mg L-1).

The strong vertical gradient in pH across the sediment-water interface (Fig. 2.8a) results from CO_2 accumulation within the sediment porewater (and in gas bubbles). As noted above, increased CO_2 shifts the pH to lower values; based upon measured CO_2 concentrations from Section 2.3 above, we predicted a pH of about 7.4. We see in Fig. 2.8a that the pH in fact approached 7.1.

The gradients in redox potential and pH were more modest in sediment cores that were not actively aerated (Fig. 2.8b). Strongly reducing conditions and lower pH values were found in the overlying water as well as in the sediments; although values were lower in the overlying water than in the aerated core, they remained higher than in the sediments. Accumulation of NH_4-N, Fe^{2+}, Mn^{2+} and sulfide, all released from the sediments, would drive the redox potential down, while CO_2 released from the sediments would also lower the water column pH. In contrast, CO_2 would not accumulate in water overlying aerated sediments since aeration would deliver O_2 that might increase CO_2 production, but also sweep CO_2 from the water, yielding higher pH conditions (Fig. 2.8).

2.5 Iron Speciation in Sediments

2.5.1 Methods

The forms of secondary iron in the sediments were evaluated using a sequential extraction procedure following DeKoff et al. (2008) that partitions Fe into Fe(III)-oxyhydroxides (as found in most surface soils), an amorphous Fe(II)S form, and the

mixed oxidation state iron sulfide greigite (Fe_3S_4). Distribution of Fe between these different forms provides key information about biogeochemical conditions in the sediments.

Sediment from the 28 sampling sites (Fig. 2.1) and from a transect between 2 adjacent diffuser lines (Fig. 2.9) were used in this investigation. Transect samples involved collection of short (10 cm) intact cores at approximately 20-30 m distance intervals between diffuser lines that were capped and returned to the lab. These cores were then sectioned into 1 cm depth intervals (0-1, 1-2, 2-3 and 3-4 cm) based in part upon microprofile measurements described in the previous section. Grab samples and core samples were extracted as described below.

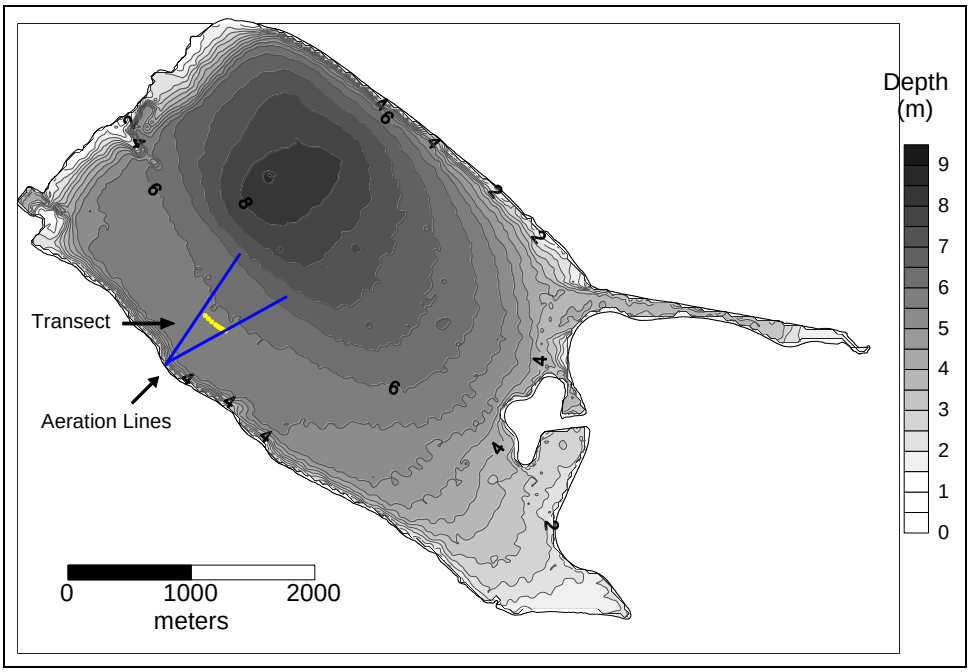

Fig. 2.9. Location of samples collected across transect between 2 adjacent diffuser lines.

Approximately 1 g samples of wet sediment (of known dry weight to yield 0.3 g d.w.) were placed into a 40 mL centrifuge tube to which was added 10 mL of a 78 g L^{-1} citrate- 9.3 g L^{-1} bicarbonate (CB) solution. The centrifuge tubes were then placed in 75 °C water bath for 10 min, shaking them twice during extraction (Dekoff et al., 2008). The CB solution has been shown to preferentially solubilize amorphous FeS from sediments (DeKoff et al., 2008). Following this extraction, the tubes were centrifuged at 4000 rpm for 10 min and the supernatant was decanted and saved for later analysis. The above

process was repeated, with the addition of 0.25 g sodium dithionite to the centrifuge tubes, shaken and returned to water bath. An additional 0.25 g sodium dithionite was added 3 additional times (total of 1 g sodium dithionite) at 10 min intervals. The sodium dithionite (Na_2S_2O4) is a powerful reductant, and is used to reduce and solubilize Fe that is in the oxidized (Fe(III)) form. Following the final addition of sodium dithionite, the sample suspensions were again centrifuged and the supernatant collected. The sediment pellets from the previous step were washed by adding 10 mL CB (no dithionite) solution to the centrifuge tubes, resuspending the sediment, then centrifuged again, and addition of the supernatant from that recovered from the sodium dithionite extraction. The sediment pellets were then washed a second time by adding 10 mL Millipure water, resuspend, centrifuged and add supernatant to that from the previous step. The final extraction involved addition of 30 mL of 1 M cold HCl to the sediment and extraction for 24 h at room temperature to recover any Fe_3S_4 (and any siderite, $FeCO_3$) present in the sediments (DeKoff et al., 2008). Siderite is not considered a likely Fe phase in Lake Elsinore sediments, however, due to the high sulfide concentrations found in the sediment pore water that would favor formation of lower solubility iron sulfides (Anderson, 2001). Extracts were diluted 1:1 with deionized water and analyzed on a Perkin-Elmer AAnalyst-800 flame atomic absorption spectrophotometer in matrix-matched standards.

2.5.2 Results

The sequential extraction procedure recovered Fe from the sediments in each of the three extractions (Table 2.8). The 1 M HCl recovered the most secondary Fe (taken as Fe_3S_4), averaging 4.50±1.23 mg g^{-1} sediment (dry-weight basis) across the 28 sampling sites, followed by CBD that dissolved Fe(III)-oxide (1.04±1.51 mg g^{-1}) and CB (amorphous FeS) (0.22±0.14 mg g^{-1}) (Table 2.8)

Table 2.8. Iron speciation in sediment collected from the 28 sediment sample locations.

	Fe Concentration (mg Fe g^{-1} d.w. sediment)		
Iron Phase	**Mean± s.d.**	**Median**	**Range**
Amorphous FeS	0.22±0.14	0.18	0.06 - 0.78
Fe(III)-Oxides	1.04±1.51	0.76	0.29 - 8.45
Fe_3S_4	4.50±1.23	4.59	1.53 - 7.34

Thus most of the secondary iron in the sediments is thought to be in reduced, sulfidic forms, accounting 84±11% of the secondary (i.e., not associated within primary minerals such as biotite) iron in the sediments. We see the labile, amorphous FeS phase accounts for a relatively modest fraction of the total iron recovered in these extractions (3.7±1.4%). Nonetheless, FeS(am) would represent a reactive phase that would contribute to the short- to mid-term oxygen demand in the sediments. Stoichiometrically, the oxidation of FeS to SO_4^{2-} and Fe^{3+} requires 2.25 O_2 molecules (Stumm and Morgan, 1980), so we estimate that about 1.2 g O_2 m^{-2} is needed to oxidize the FeS(am) in the upper 1 cm of the sediments. The rate for this oxidation reaction is not known, so it is not possible to quantify its contribution to overall SOD, but this nevertheless represents an inventory of reduced matter that needs to be oxidized in order to maintain fully oxic conditions at the sediment-water interface. That some Fe(III)-oxides remain in the sediments suggest complicated redox and precipitation reactions are present. Overall, FeS(am) is thought to represent a relatively modest fraction of the total SOD in the sediments compared to active microbial respiration and decomposition reactions.

The inventory of Fe_3S_4 is much larger than either the FeS(am) or Fe(III)-oxide pools (Table 2.8). Greigite is a mixed oxidation state mineral, with one Fe(II) and two Fe(III) atoms in the mineral. Assuming the sulfide associated with this mineral is also exerting a demand on O_2 near the sediment-water interface, one calculates a much higher amount of O_2 needed to fully oxidize this mineral (68.6 g O_2 m^{-2}).

The distribution of these three Fe phases shared common features, with a site of high concentrations of all three minerals present near the northwestern corner of the lake (Fig. 2.10). A region of higher FeS(am) was also present near the San Jacinto River inflow (Fig. 2.10a). Similar trends in distribution were found in the Salton Sea, where Fe sulfides were often associated with riverine input of suspended sediment eroded from the watershed (DeKoff et al., 2008).

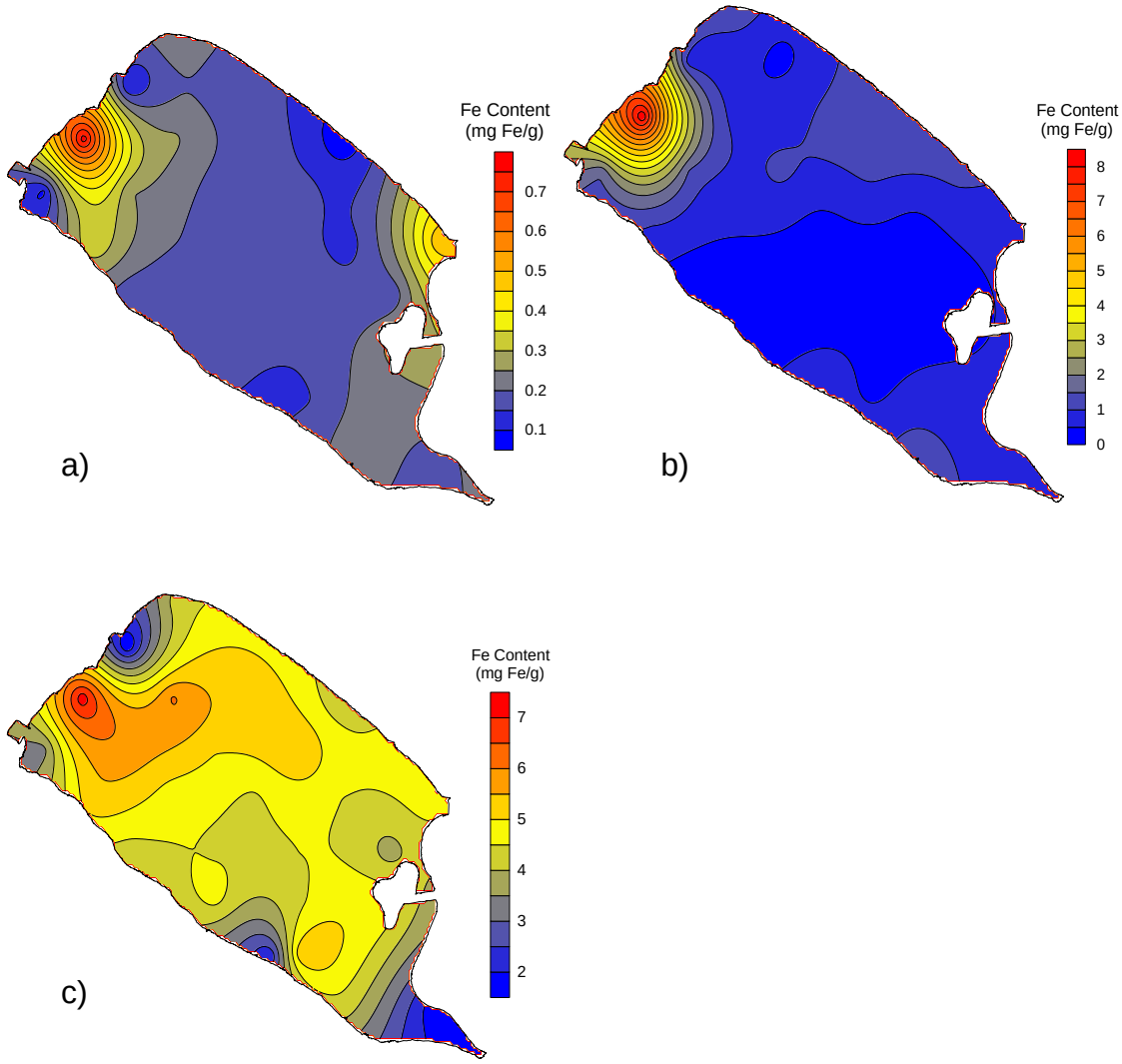

Fig. 2.10. Distribution of different forms of iron across the lake: a) FeS(am), b) Fe(III)-oxides, and c) Fe_3S_4.

The distribution of iron species vertically with depth and as a function of distance from the diffuser lines was also evaluated. The concentration of FeS(am) recovered in the CB extractant exhibited a weak but consistent downward trend with depth, decreasing by approximately 25-30% at the 3-4 cm depth interval when compared with the 0-1 cm surface layer (Fig. 2.11a). There was no clear trend with distance from the diffuser lines. The Fe(III)-oxide phase exhibited the inverse trend, with somewhat lower concentrations near the surface and slightly higher values further in the sediments (Fig. 2.11b). Fe_3S_4 contents also tended to increase with depth (data not shown).

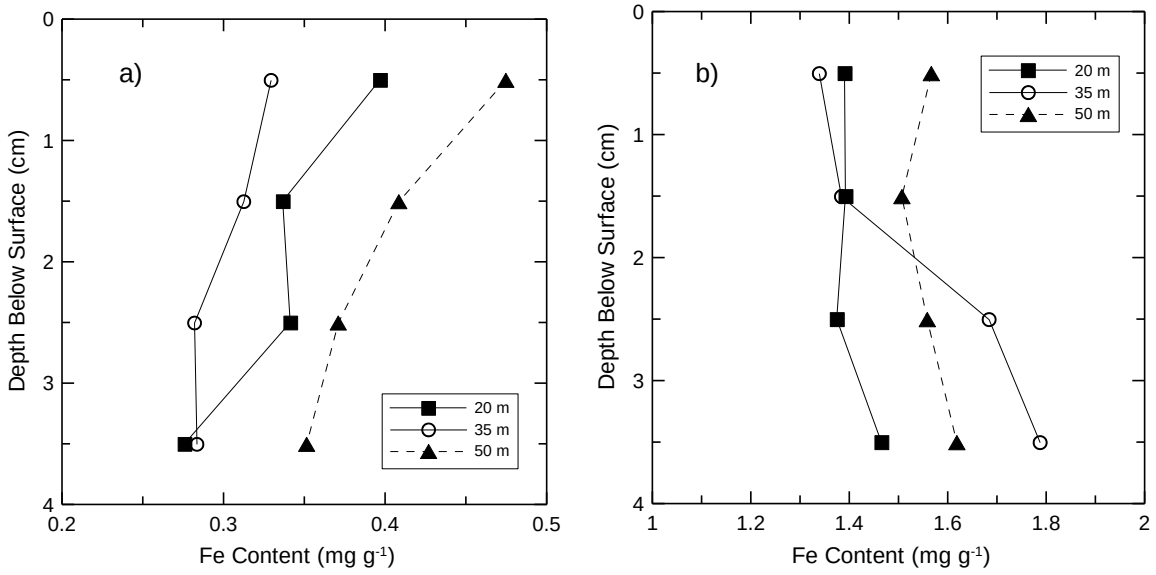

Fig. 2.11. Concentration of Fe species with depth below the sediment surface at 20, 35 and 50 m from the nearest diffuser line: a) FeS(am) and (b) Fe(III)-oxides.

The concentration of the different Fe species in the uppermost 1 cm as a function of distance from diffuser lines can be seen more clearly in Fig. 2.12. Concentrations of all three phases, including the Fe(III)-oxide, increased slightly as a function of distance from adjacent diffuser lines (Fig. 2.12a). Somewhat different behavior might have been hoped for, *i.e.*, higher levels of Fe(III)-oxides and lower concentrations of FeS and Fe_3S_4 immediately adjacent to the diffuser lines. Such an observation would have provided direct geochemical evidence for sufficiently high DO concentrations as a result of aeration to maintain Fe(III)-oxides and thus limit PO_4-P release from the sediments.

The color of the surface sediments was also quantified using Munsell Soil Color Charts. The body of the sediments exhibited uniform 10Y 3/1 color (very dark greenish gray color) (Fig. 2.13a), indicative of strongly reducing conditions, while the surface layers were generally 2.5Y 3/2 (Fig. 2.13b). In contrast, the upper 1-3 mm of intact cores vigorously aerated for several days turned lighter and browner, generally 2.5Y 4/3 to 2.5Y 6/6 (Fig. 2.13b), indicative of oxidizing conditions with Fe(III)-oxides and Fe(III)-oxyhydroxides present. Based upon sediment Fe speciation and observations concerning sediment color, little evidence exists for favorably oxic conditions being maintained near the aeration diffuser lines. This is, no doubt, a result of the very high WOD and SOD rates in the lake (section 2.2.).

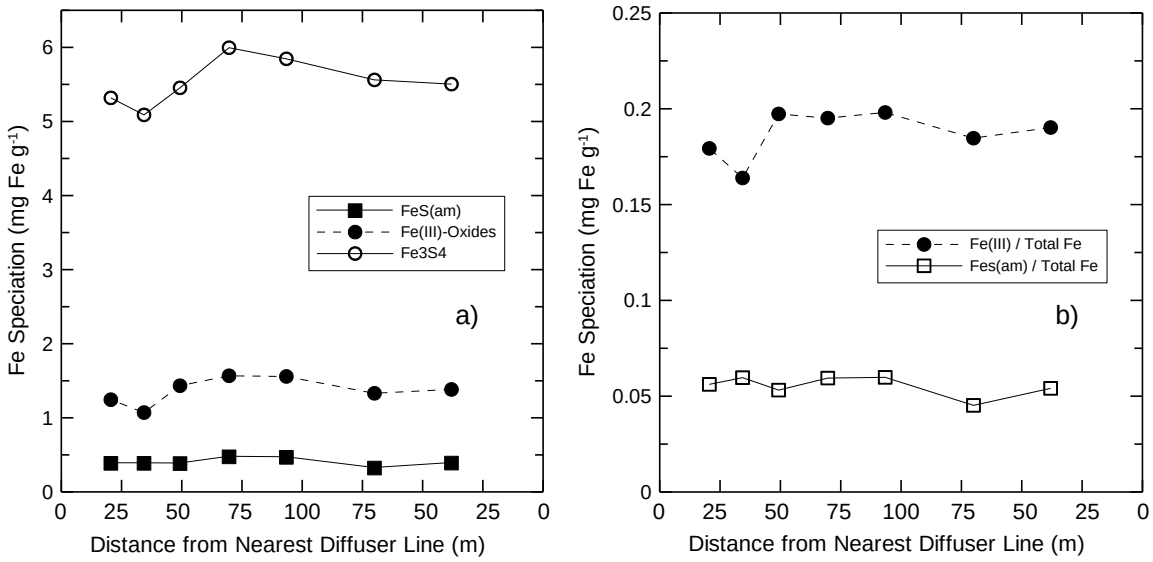

Fig. 2.12. Fe speciation in top 1 cm of sediment as function of distance from nearest diffuser line: a) concentrations and b) ratio of FeS(am) and Fe(III)-oxides to total secondary Fe.

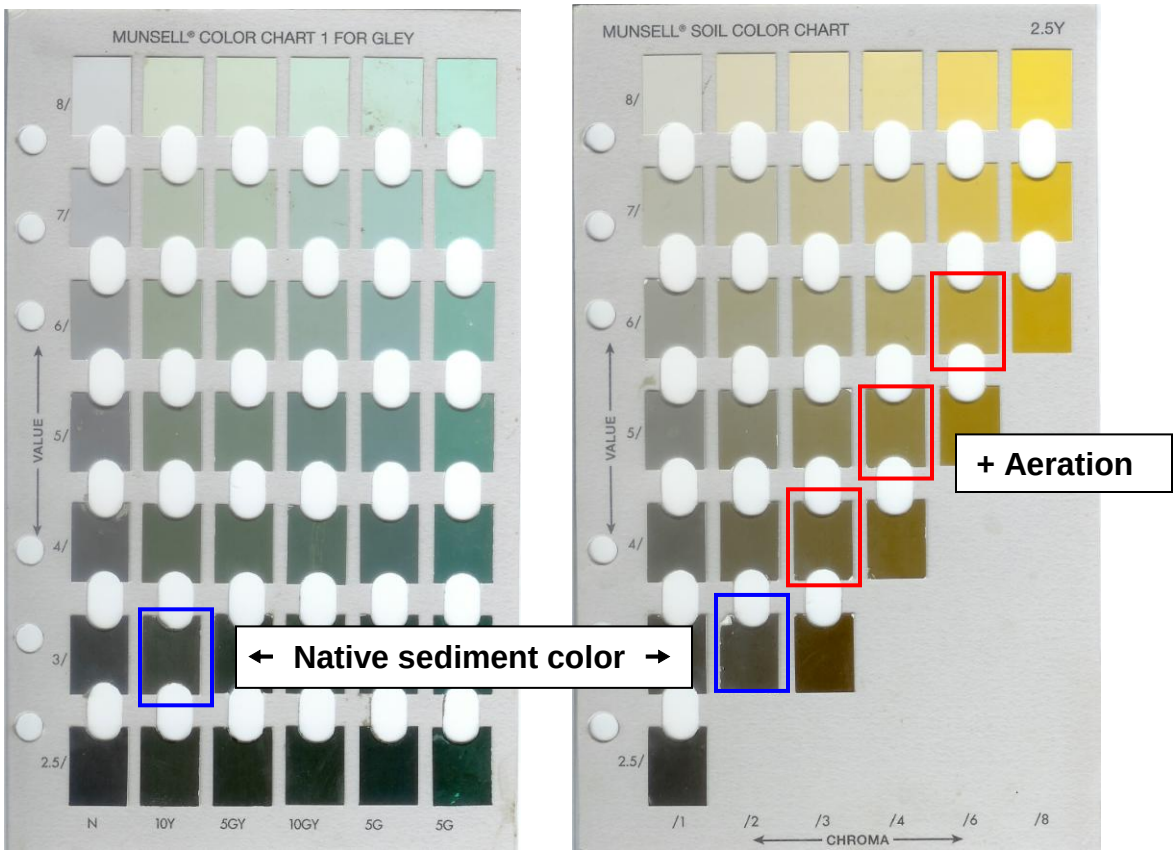

Fig. 2.13. Munsell color charts showing colors of native and aerated sediments.

3. BATHYMETRIC SURVEY & HYDROACOUSTIC SEDIMENT CHARACTERIZATION

Available information about the bathymetry of Lake Elsinore is based largely upon depth measurements made at 49 sediment sampling sites (Anderson 2001). While providing a detailed characterization of the sediments at these sites, the limited number of measurements in that study provide only a very coarse representation of the basin characteristics. Much more detailed bathymetric information can be determined using hydroacoustic survey techniques.

In addition to depth to sediments, hydroacoustics can also provide information about sediment properties, including hardness, roughness (Chivers et al., 1990) and texture (BioSonics, 2008). It is recognized that sediment characteristics strongly influence nutrient loading, oxygen demand, susceptibility to resuspension, spawning and benthic habitat quality in lakes. As a result, a detailed multifrequency hydroacoustic survey was conducted in June-July 2010. Data files were also shared with ReMetrix for development of a visualization tool for Lake Elsinore.

3.1 Methods

A bathymetric survey and hydroacoustic sediment characterization was conducted using a BioSonics DT-X echosounder with 430-kHz and 38-kHz single beam transducers with integrated pitch-roll sensors multiplexed with a 201-kHz split beam transducer. The 430-kHz echosounder has a small near-field and has low acoustical penetration of bottom sediments, thus offering a very accurate way of determining sediment depth and acoustical properties (e.g., hardness, roughness, texture) of the surficial sediments. The lower frequency of the 38-kHz echosounder, in contrast, has much lower absorption by bottom sediments and can thus be used in some settings to determine sediment thickness (Elci et al., 2009). Penetration depths into fine organic sediments can be several meters, until the sound wave is reflected off of a strong density contrast such as granite bedrock or a compacted clay lens or desiccation layer. The 201-kHz frequency transducer provided a unique, 3rd acoustic signature of the bottom sediments.

Bathymetric and acoustical characterization of the bottom sediments in Lake Elsinore was conducted on a regular grid with a nominal 100 m spacing and survey speed of 3-4 knots (Fig. 3.1). Data was acquired at 5 pings per second (pps) on each of the 3 frequencies covering more than 270 km (170 miles) of transects across the lake. Each of the 3 transducers was calibrated using tungsten-carbide calibration spheres

every day in the field prior to collection of acoustic data and at the end of the day's survey. Surveys were conducted between 7 a.m. and 3 p.m. on June 28-30 and July 12-14 during periods of relatively calm conditions on the lake. Echograms were analyzed using BioSonics Visual Bottom Typer (VBT) v. 1.12 (Seattle, WA). Acoustical properties were averaged over 20 pings using 30 log R time-varied gain with depth-normalization. Georeferenced hydroacoustic data, collected with a JRC 212W realtime DGPS, was subsequently used to develop a detailed bathymetric map for the lake, and maps of sediment acoustical properties.

Acoustical properties were then correlated with organic C content, porewater nutrient concentrations (section 2.1), and rates of nutrient release and oxygen demand (section 2.2). Sediment thickness was measured at the 28 sites using a universal percussion corer.

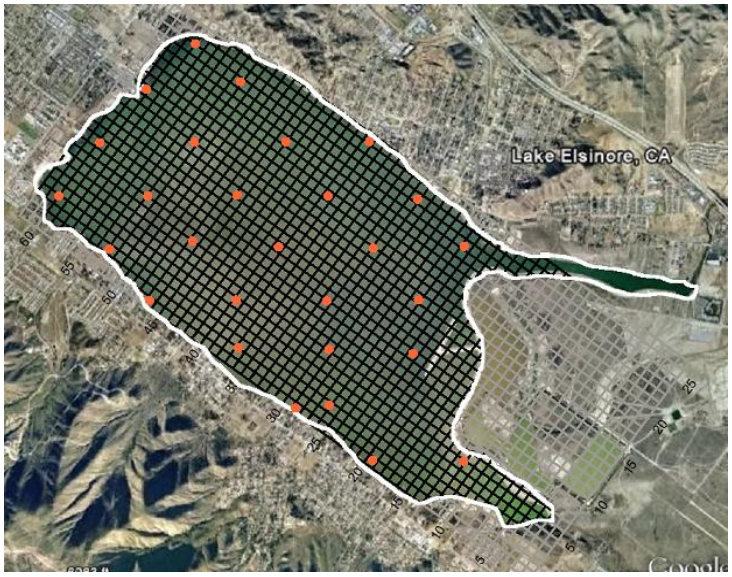

Fig. 3.1. Hydroacoustic survey grid and sediment sampling locations.

3.2 Results

3.2.1 Bathymetry

The depth at any location on the lake is measured by the time it takes for a pulse of sound emitted from the echosounder transducer to travel to the lake bottom and be returned as a bottom echo. The travel time is then converted to distance from the known speed of sound in water after correction for temperature, salinity and pH (approximately

1500 m s^{-1}) (Luxton, 2002). The echograms show very clearly the strong acoustic backscatter from bottom sediments, although fish and zooplankton, as well as larval aquatic insects and gas bubbles, also reflect sound (e.g., Fig. 3.2). The strength of the backscatter from objects suspended within the water column is a function of the size and density contrast with water. In a related way, the density, hardness and roughness of bottom sediment influences the strength of the bottom echo.

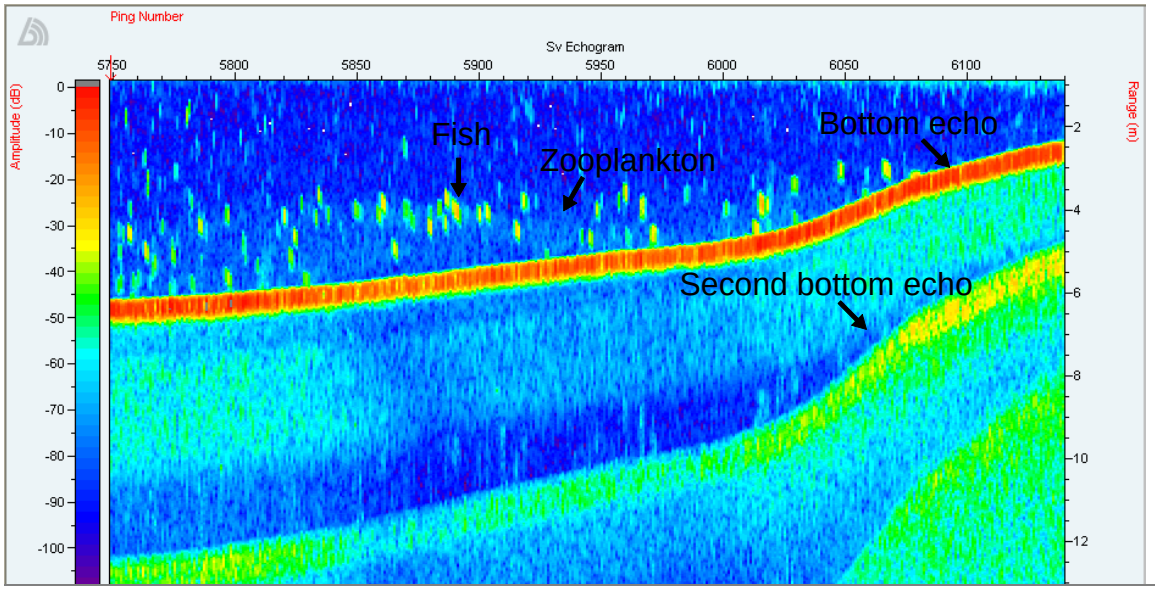

Fig. 3.2. Example echogram (201-kHz) showing strong bottom echo as red band of varying depth (echo strength shown on color scale on left hand side of figure, from 0 to –120 dB); 2nd bottom echo that results from bottom echo being reverberated from lake surface that is again backscattered from bottom sediments before being measured by echosounder (shown at 2x range of bottom echo, right hand side of figure); discrete fish targets; and diffuse backscatter from zooplankton cloud.

The latitude, longitude and depth, after correction for distance of transducer face below water surface, were imported into Surfer software program (Golden Software) and geostatistically interpolated using kriging to develop a bathymetric map for the lake (Fig. 3.3; also Fig. 2.9). Since the lake level varies so strongly, elevation contours are shown (2 ft intervals). The deepest location (elevation of 1214') is found at 33.6683º N, -117.3569º W immediately below the axial flow pumps located at DS-1 (Fig. 2.3). One in fact notes small regions of lower bottom elevations at each of the five docking stations relative to nearby locations, reflecting the scouring and mechanical displacement of approximately 1-2' of bottom sediments as a result of pump operation (Fig. 3.3).

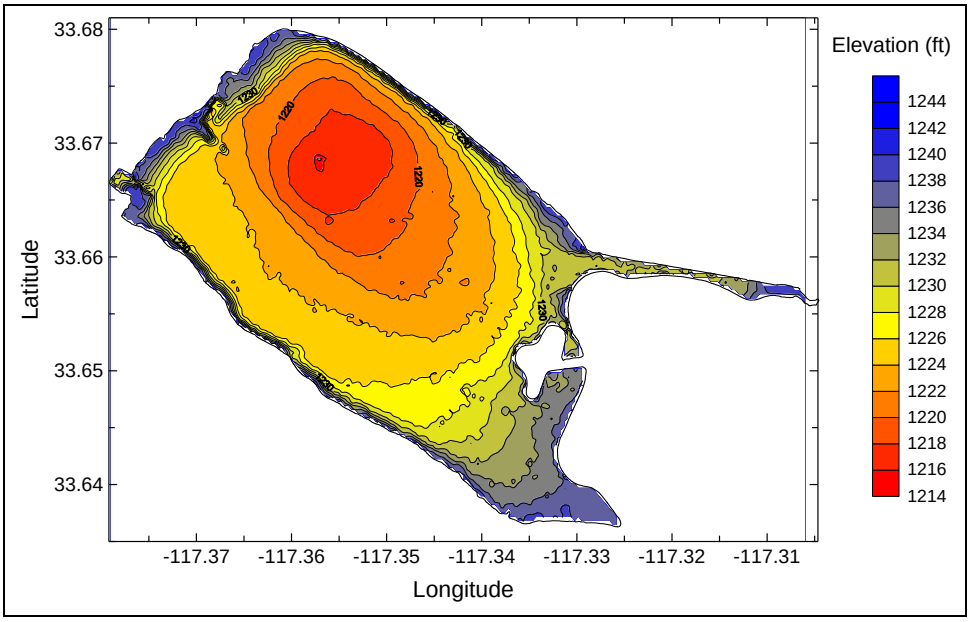

Fig. 3.3. Map showing basin elevation as a function of latitude and longitude.

This bathymetric map provides much greater spatial detail and significantly improved precision in the depth measurements than the map developed from limited measurements made in 2000-01 (Anderson, 2001), although general agreement exists between the two maps. Elevation-area-volume relationships based upon these survey results are being developed by ReMetrix and have thus not been included in this report.

3.2.2 Sediment Acoustical Properties

As described above, the strength and waveform of the bottom echo reflects the properties of the bottom sediments. Variations in the strength of the bottom echo across the sediments can be seen, *e.g.*, in Fig. 3.4a, where strong backscatter (-5 to -10 dB) was found in relatively shallow water down to about 5 m depth (shown as range on y-axis on right-hand side of figure). A short distance further into the lake, where the bottom elevation flattens out to a depth near 6 m (pings #7220-7300), one notes reduced backscatter strength (~-20 dB), before increasing somewhat further into the lake (e.g., pings #6920-7000) (Fig. 2.4a). Broadly similar trends were also observed at 201-kHz (Fig. 3.4b). These changes in backscatter strength reflect in a complex way variations in sediment physical properties.

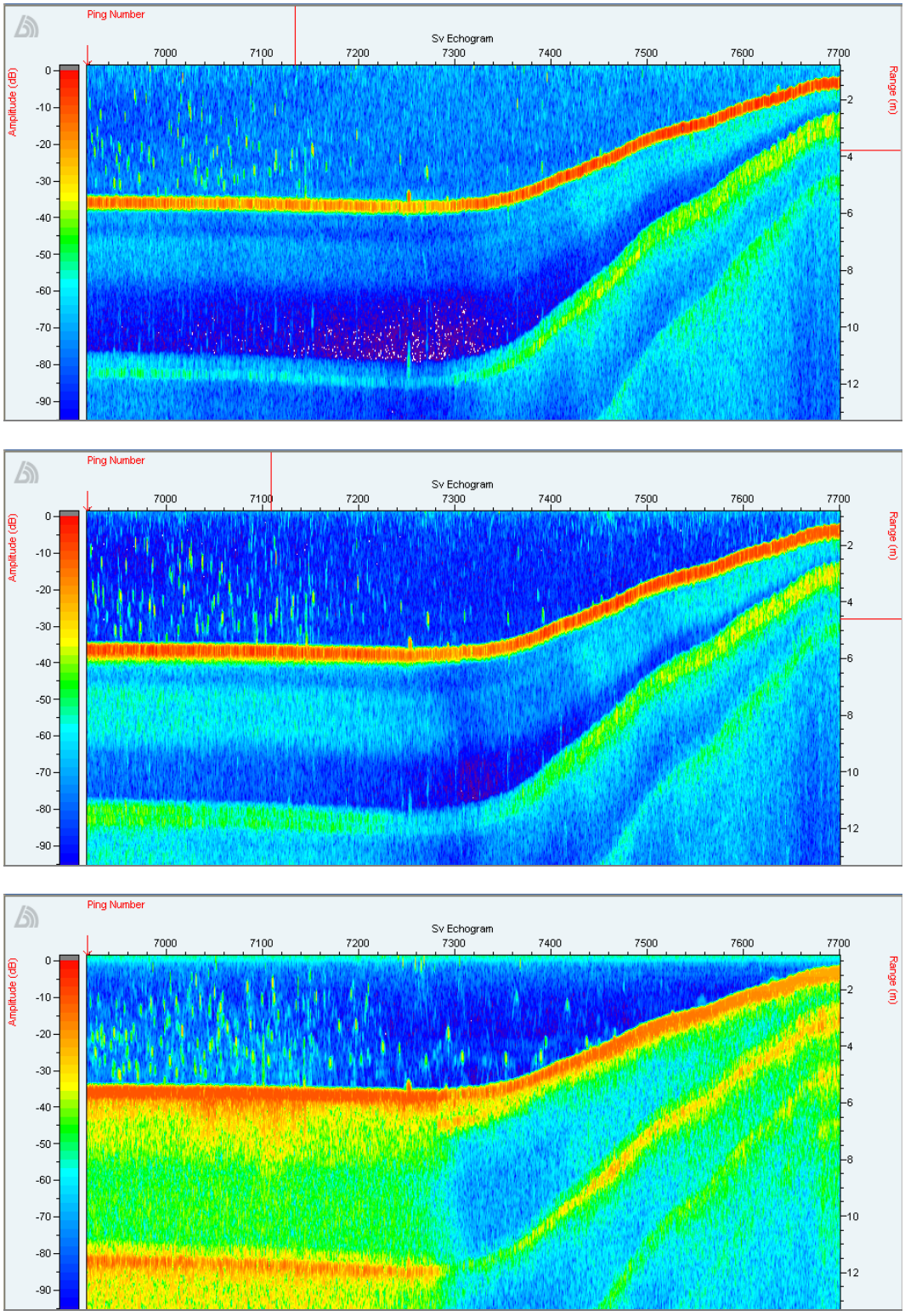

Fig. 3.4. Echograms showing different frequency-dependence of backscatter and bottom echo: a) 430-kHz, b) 201-kHz and c) 38-kHz.

At the same time, absorption by sediments (and water) varies with the frequency of sound, with lower frequency sound waves (*e.g.*, 38-kHz) exhibiting less absorption and greater penetration into sediments than higher frequencies (*e.g.*, 430-kHz). This can also be seen in example echograms at 38, 201 and 430-kHz (Fig. 3.4).

The "thickness" of the reddish band in the echograms associated with the bottom echo was modest at 430-kHz (Fig. 3.4a) and slightly thicker at 201-kHz (Fig. 3.4b), with evidence of regions of significant penetration at 38-kHz (*e.g.*, ping #7020-7140 in Fig. 3.4c.) Heterogeneity of thickness of bottom sediments clearly exists, with generally acoustically "thin" sediments in shallower water, and thicker sediments located in deeper regions of the lake that results from sediment focusing.

Four distinct acoustical properties were extracted by VBT from echograms: the integral of backscatter strength (E0), the strength of the 1st part of the 1st bottom echo (E1'), the strength of the 2nd part of the 1st bottom echo (E1), and the strength of the 2nd bottom echo (E2). The fractal dimension of the bottom echo appears to hold the greatest utility for characterizing bottom (BioSonics, pers. comm.) (Fig. 3.5).

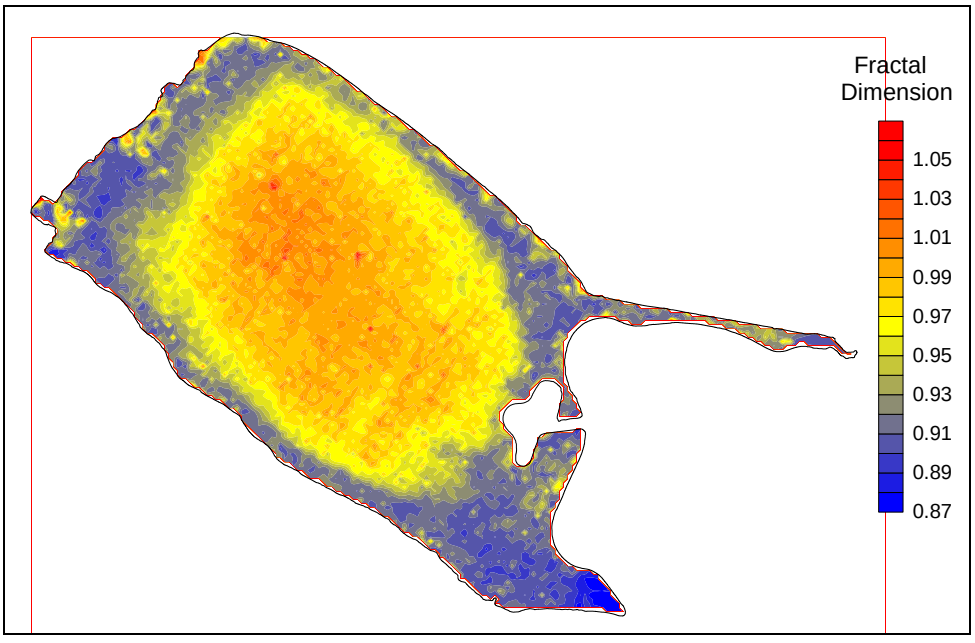

Fig. 3.5. Map showing fractal dimension of bottom echo (430-kHz).

The fractal dimension was found to be relatively low near the margins of the lake, and increased to values approaching or exceeding 1 near the center of the lake (Fig. 3.5), generally following trends in depth (Fig. 3.3).

The utility of the fractal dimension of the bottom echo and other acoustical properties is evaluated based upon ground-truthing of the acoustical data. Owing to the central role that organic C plays in nutrient recycling, sediment oxygen demand, and other biogeochemical processes, acoustical properties measured at our 28 sediment sites were regressed against measured organic C concentrations. The fractal dimension of the bottom echo was consistently the most strongly correlated of any of the acoustic properties with organic C. The r value for the fractal dimension at 430-kHz (r=0.91) was the highest of the three frequencies and accounted for 83% of the variance in observed organic C concentrations in the 28 sediment samples. Organic C content could be estimated following the equation:

$$\% \text{ Organic C} = 43.69 * \text{Fractal Dimension} - 38.86 \qquad (3.1)$$

Table 3.1. Correlations between organic C concentration and different acoustic properties and wavelengths. An r-value >0.478 is statistically significant at p=0.01.

Property	430-kHz	201-kHz	38-kHz
E0	0.20	0.16	-0.23
E1	0.18	0.74	0.78
E2	-0.18	0.49	0.66
E1’	0.35	0.74	0.78
FD	0.91	0.86	-0.84
E1/E2	0.30	0.14	-0.48
E1’/E1	0.46	0.50	0.01
E1/FD	0.14	0.72	0.78

Based upon eq 3.1 and measured fractal dimensions at 430-kHz (Fig. 3.5), we can develop a map showing the distribution of organic C across the lake (Fig. 3.6). The margins of the lake are thus projected to have generally low organic C contents (<1 %), with much of the center of the basin having concentrations of 3.5 – 5.5% (Fig. 3.6). Rather little sediment with intermediate organic C contents (1-3%) was found.

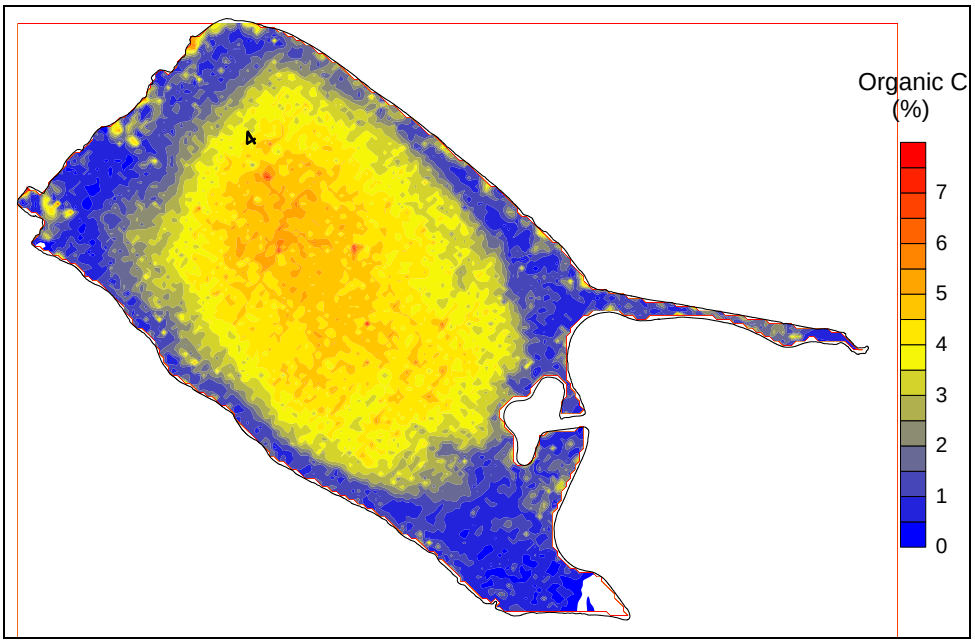

Fig. 3.6. Distribution of organic C content of sediments across the lake.

The strong correlation between organic C concentration and SOD (eq 2.1) also allows us to estimate the distribution of SOD across the lake (Fig. 3.7). Low organic C content sediments near the lake margin were predicted to have SOD values <0.3 g m^{-2} d^{-1}, with other deeper regions exceeding summer SOD rates of 1 g m^{-2} d^{-1}.

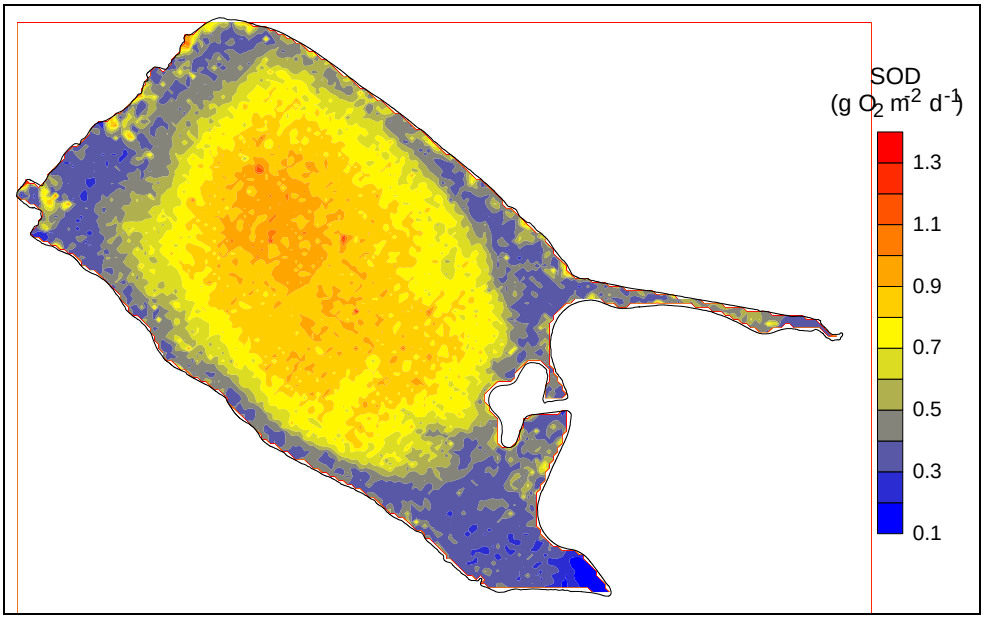

Fig. 3.7. Distribution of SOD across the lake (summer maximum values).

This spatial information not only indicates where O_2 depletion is likely, but also allows one to estimate the total, lake-wide SOD. This then tells us the amount of O_2 that needs to be supplied to the lake through the combination of photosynthetic O_2 production, natural reaeration from the atmosphere, and artificial mixing/aeration to maintain oxic conditions across the basin.

Based upon Fig. 3.7, we calculate a total lakewide SOD in August of 7600 kg O_2 d^{-1}. The rate of net O_2 production in the photic zone measured in *in situ* light-dark bottle experiments from the biological monitoring program on August 19 was 2.08±0.53 mg L^{-1} h^{-1}. (The photic zone is taken here as 2x the Secchi depth, which at that time was 0.35-0.4 m, for a zone of active photosynthesis of about 0.8 m) The total net photosynthetic O_2 production was then calculated as the product of the net O_2 production rate multiplied by the volume of the photic zone ($9.7x10^6$ m^3) and the duration of strong light input to the lake surface (approximately 10 h d^{-1}); after correction for respiratory losses at night (32,592 kg O_2), we estimate a potential net daily photosynthetic O_2 input of 169,168 kg d^{-1}. The rate of WOD measured in the core-flux studies described in section 2.2 (1.65±0.23 mg L^{-1} d^{-1}) was multiplied by the volume of water below the photic zone ($5.66x10^7$ m^3) to yield an additional loss of O_2 of 93,406 kg d^{-1} (Table 3.2). These calculations indicate that, theoretically, about 1.7x the total O_2 demand in the lake in August 2010 could be met if O_2 from photosynthesis was efficiently mixed throughout the water column. One also notes that SOD contributed a relatively small amount to the overall O_2 demand when compared with WOD (Table 3.2).

Table 3.2. Dissolved oxygen balance for Lake Elsinore: August 2010.

	kg O_2 d^{-1}	**"Algal Crash"**
Net O_2 Production in Photic Zone	+169,168	+35,488
Net WOD below Photic Zone	-93,406	-93,406
Net SOD	-7,600	-7,600
Balance	+68,162	-65,518

Stratification, of course, limits the downward transport of DO. The DO concentration in the surface layer is a function of *in situ* O_2 production and consumption, loss to the atmosphere through volatilization, and downward mixing/dilution. The relative magnitude of each of these processes governs the overall DO concentration in the water.

Biological conditions can also shift *in situ* production and loss rates. For example, one can readily see that a reduction in photosynthetic production, to levels measured on June 22, 2010 (light bottle O_2 production rate of 0.64±0.12 mg L^{-1} h^{-1}), could result in a net deficit assuming WOD and SOD values remained unchanged (Table 3.2).

The relationship between PO_4-P flux from sediments and their % organic C content (Fig. 2.5a) allow one to also map out the zones where internal loading is greatest (Fig. 3.8). Based upon core-flux measurements, coarse-textured sediment with very low organic C contents potentially serve as net sinks for PO_4-P, although most of sediments in the lake serve as significant sources under low to moderate DO concentrations (Section 2.2). One notes that this distribution is broadly similar to the type classification (Types I, II, and III) made earlier (Anderson, 2001).

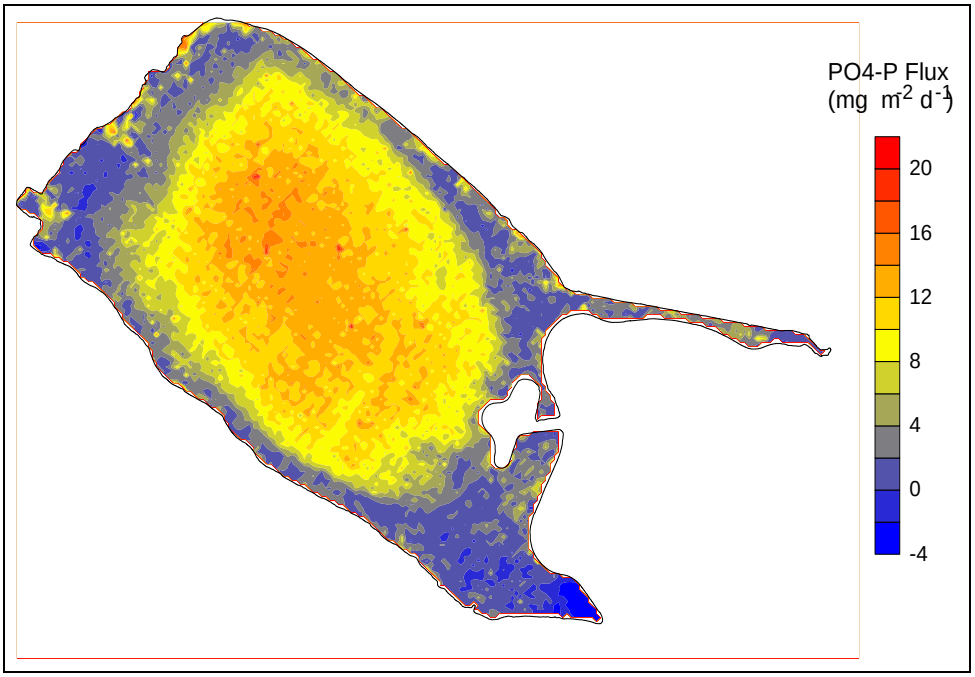

Fig. 3.8. Map showing distribution of summer PO_4-P nutrient release rates across lake.

The total area of lake sediments contributing PO_4-P to the water column at a given rate is shown in Fig. 3.9a. Thus we see that about 300 acres of the lake have an internal loading rate of 1-2 mg m^{-2} d^{-1}, with a slightly greater area possessing a flux rate of 11-12 mg m^{-2} d^{-1} (Fig. 3.9a). The product of area and flux rate allows one to calculate

the mass of PO_4-P contributed by each region.. Summed across the basin, 85.8 kg d^{-1} of PO_4-P is estimated to be delivered (in the summer) from the sediments to the overlying water. One-half of the total PO_4-P internal loading comes from 550 acres (about 19% of the total sediment area) with flux rates exceeding 11 mg m^{-2} d^{-1}. Control of internal loading from this portion of the sediments would provide the most efficient way to improve water quality.

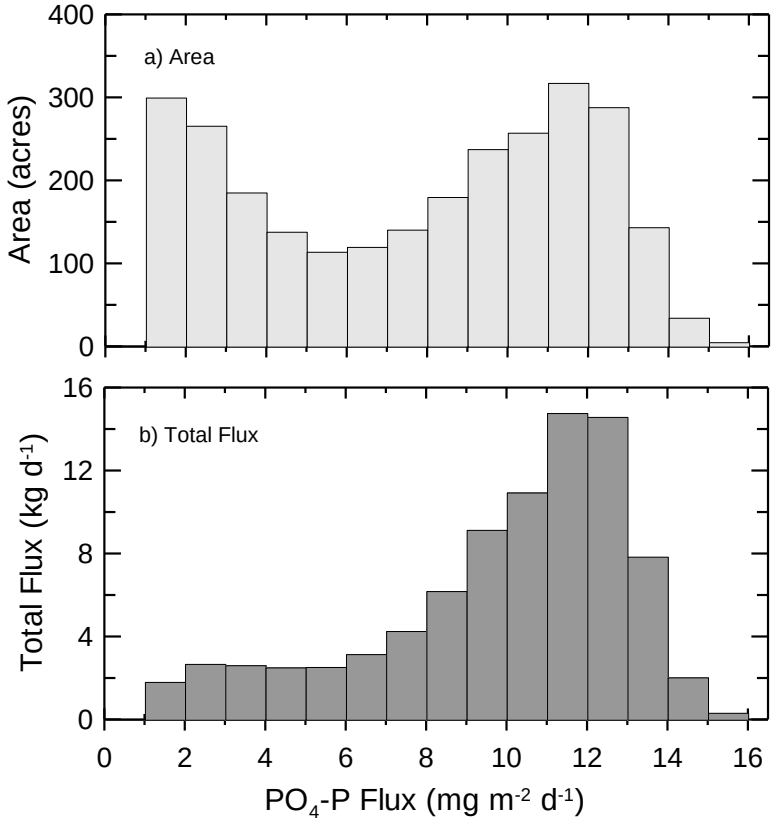

Fig. 3.9. Flux of PO4-P from the sediments: a) area and b) total mass per day.

A similar spatial representation is provided for NH_4-N flux from the sediments (Fig. 3.10), with much higher internal loading rates near the center of the lake (>100 mg NH_4-N m^{-2} d^{-1}) and lower rates near the margins. The very southern tip of the lake was not surveyed, so this region represents an extrapolation beyond the measurement range (for all other plots as well).

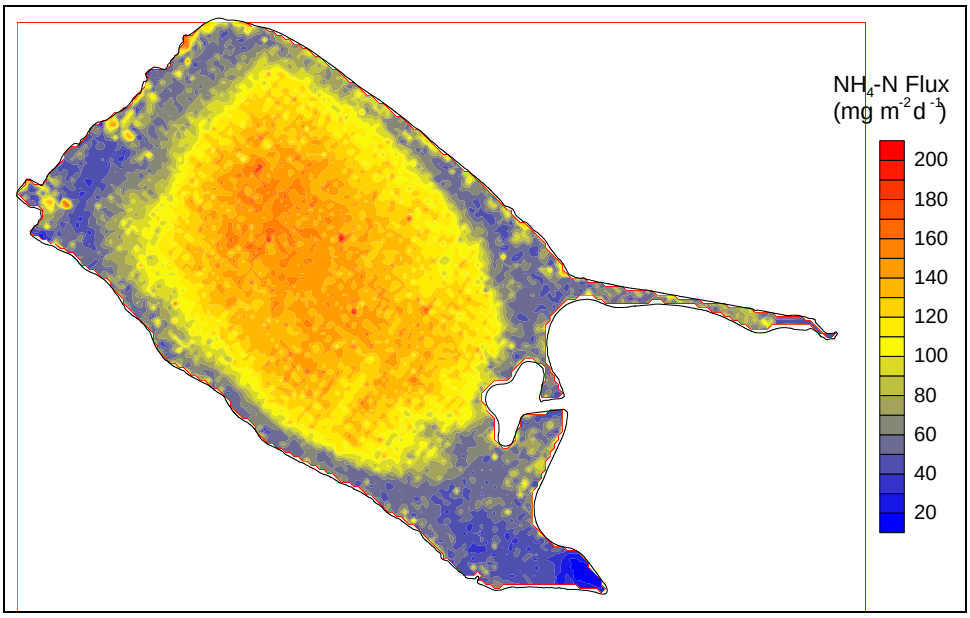

3.10. Map showing distribution of summer NH_4-N nutrient release rates across lake.

In addition to nutrients released from bottom sediments, echograms clearly show release of gas bubbles from fine organic sediments within the lake (*e.g.*, Fig. 3.11). With little drift by the boat during acquisition of data, bubbles rising vertically are seen as off-axis linear streaks (Ostrovosky et al., 2008). The deviation from vertical reflects the ping rate, movement of the transducer (boat) over rising bubble(s), and horizontal displacement by advective water currents. (Fish motion would typically be oriented more horizontally with random velocities and directions. Thus, the acoustic targets with little motion are thought to be generally small fish.)

Knowing the ping rate (5 pps), the angle of the rising bubble, and other geometric factors, we estimate a bubble rise velocity of 0.25 m s^{-1}. This rise velocity is consistent with a bubble volume of about 0.001 cm^3 and diameter of approximately 1.2 mm (Ostrovosky et al. (2008). Knowing the 201-kHz transducer beam half-angle (6.6º) and depth to the sediments (approximately 5 m), one can further infer an in situ ebullition rate potentially as high as 0.002 bubbles m^{-2} s^{-1}. Assuming 75% of the lake area has sufficient organic matter to generate significant gas production (e.g., Figs. 2.6, 2.7), this translates to up to $2x10^{10}$ bubbles d^{-1} emitted from the sediments, corresponding to a gas flux of 15,000 L d^{-1}. At a CO_2 concentration in the bubbles of 65 mg L^{-1} (assuming limited loss to the water column during transport), potentially up to 1 kg CO_2 may be exported from the sediments of Lake Elsinore each day. For comparison, based upon

net O_2 production in the photic zone of 169,168 kg d^{-1}, one estimates CO_2 uptake by phytoplankton near 232,606 kg d^{-1}; these numbers suggest that < 0.001% of the CO_2 taken up through net primary production is lost from the lake through gas ebullition. The sediments of Lake Elsinore thus appear to be a very effective sink for atmospheric CO_2.

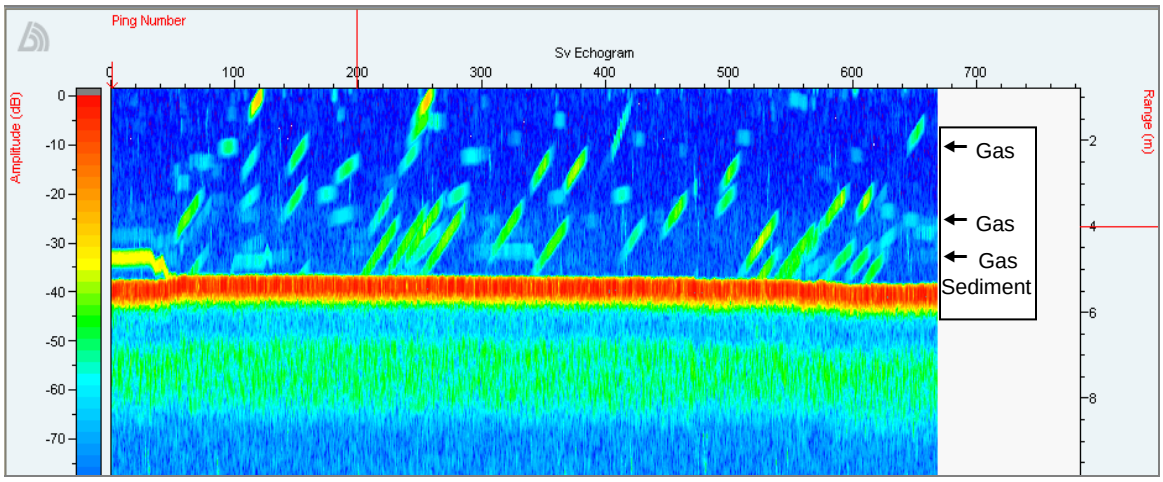

The potentially more significant effect of gas ebullition is on water quality in the lake; ebullition can enhance nutrient release from sediments relative to simple diffusive flux. Observations that core-flux measurements of internal loading consistently exceeded, by a large margin, diffusive flux rates from peepers (Anderson, 2001), provides some indirect evidence for ebullition and other transport processes within the sediments.

4. RETROSPECTIVE REVIEW AND STATISTICAL ANALYSIS OF WATER QUALITY DATA

A significant body of monitoring data have been collected for Lake Elsinore over the past decade. These data were reviewed here with the goal of developing of statistical relationships to understand the dominant drivers of water quality (especially chlorophyll a concentrations). Importantly, this time period includes periods of pronounced drought, resulting in increased salinities and lower lake levels, as well as El Nino events with large freshwater inputs generally high in dissolved nutrients.

4.1 Water Quality Conditions: 2000 - 2009

It is well-recognized that water quality in Lake Elsinore has varied markedly over the past decade. Chlorophyll a concentrations have ranged from <10 $\mu g\ L^{-1}$ on at least one sampling date during the winters of 2001 and 2005-2008, to values in excess of 300 $\mu g\ L^{-1}$ in late summer-fall of 2002-2004 (Fig. 4.1).

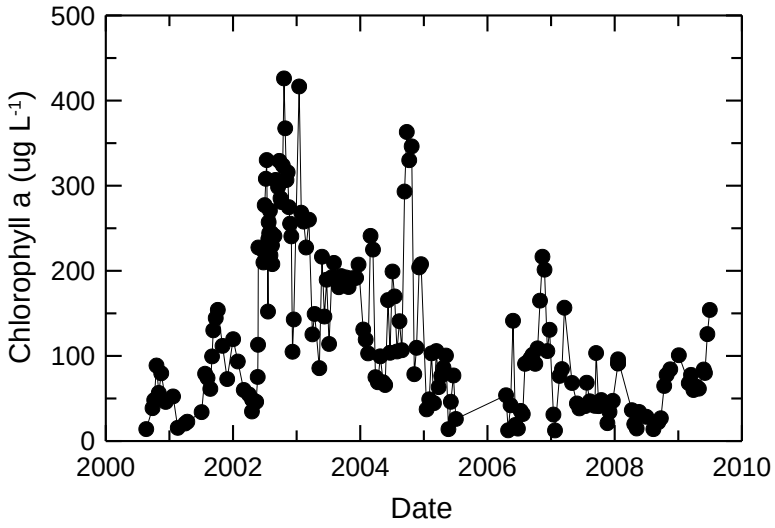

Fig. 4.1. Chlorophyll a concentrations in lake from 2000-2009 (surface samples collected from near center of lake, site 9 or E2 in most studies).

Total nitrogen and phosphorus concentrations exhibited strong seasonal and interannual variations as well. Total P increased from values <0.1 mg L^{-1} in 2000 to

values >0.5 mg L^{-1} in 2003-2004 (Fig. 4.2). Concentrations decreased beginning in 20005 and have more recently ranged from about 0.1 – 0.2 mg L^{-1} (Fig. 4.2).

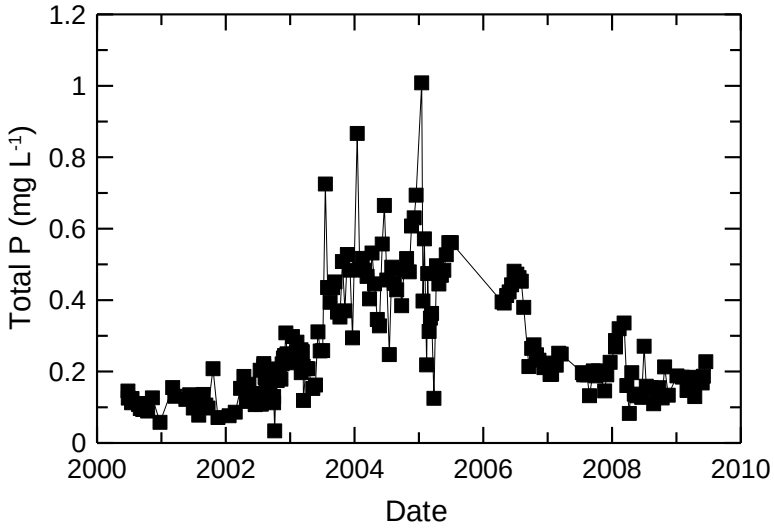

Fig. 4.2. Total P concentrations in lake from 2000-2009 (depth-integrated samples collected from near center of lake, site 9 or E2 in most studies).

Total N concentrations followed similar trends, increasing from about 2 mg L^{-1} in 2000 to concentrations sometimes in excess of 7 mg L^{-1} in 2004 (Fig. 4.3).

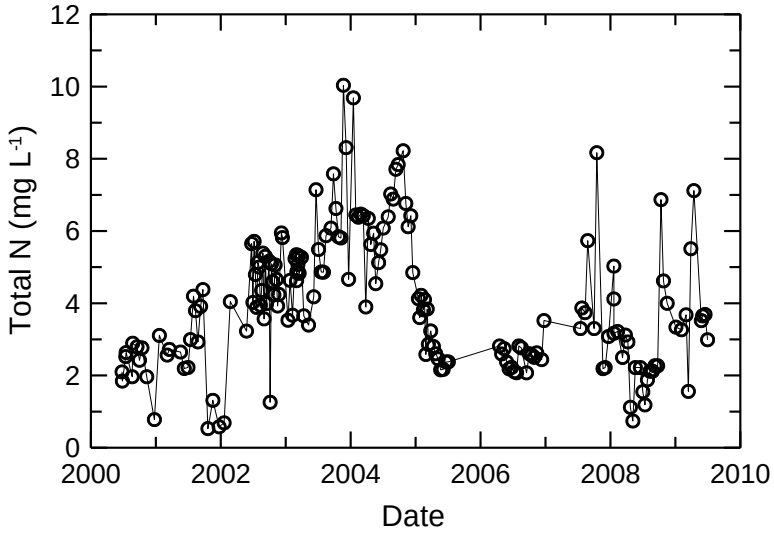

Fig. 4.3 Total N concentrations in lake from 2000-2009 (depth-integrated samples collected from near center of lake, site 9 or E2 in most studies).

The near-record runoff in the winter of 2005 dramatically reduced total N concentrations in the lake; within a period of a couple months, TN concentrations declined from 8 mg L^{-1} to almost 2 mg L^{-1} (Fig. 4.3). Concentrations remained modest in 2006 but have been more variable over the past couple of years, generally at levels of 2-4 mg L^{-1}.

The TN:TP ratio has accordingly also varied strongly over the past decade (Fig. 4.4). Ratios suggesting strong P-limitation have been seen, as well as intervals in 2005-2006 where N-limitations might be inferred, although the overall availability of nutrients have generally been sufficiently high that light or other limitations are thought to be more important in regulating algal productivity in the lake. For example, periods of low dissolved Si are traditionally seen during the spring, likely serving as a limitation to diatom production.

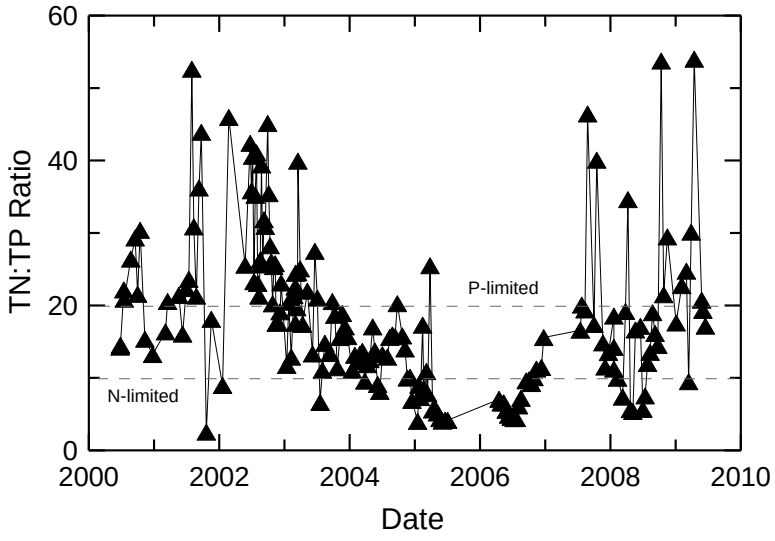

Fig. 4.4. TN:TP ratio in lake from 2000-2009 (depth-integrated samples collected from near center of lake, site 9 or E2 in most studies).

With large evaporative losses from the lake each summer, combined with winters of limited rainfall and periodic El Nino events, TDS concentrations have varied as well (Fig. 4.5). TDS concentrations increased approximately exponentially during the drought of 2000-2002 to values over 2200 mg L^{-1}, before decreasing following rainfall and runoff in 2003 to about 1400 mg L^{-1}, and declining further in 2005, to about 800 mg L^{-1} (Fig. 4.5). TDS concentrations increased from 2006-2007 and remained around 1600 mg L^{-1} into the summer of 2009.

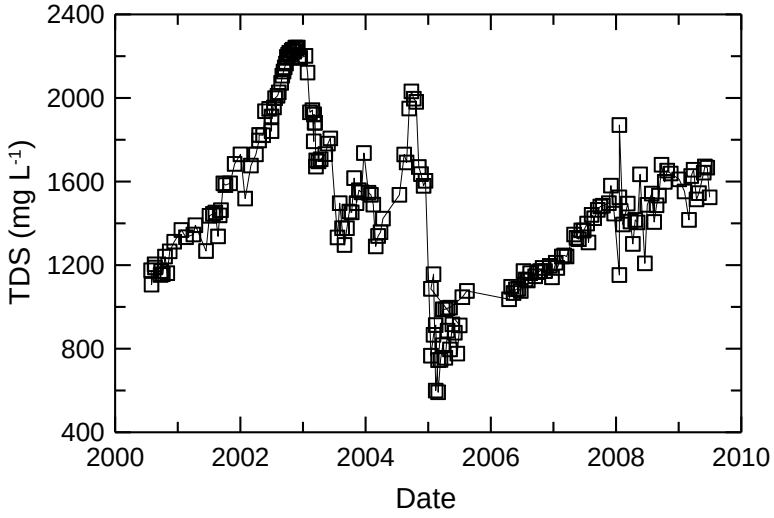

Fig. 4.5. TDS concentrations in lake from 2000-2009 (depth-integrated samples collected from near center of lake, site 9 or E2 in most studies).

To reduce the "noise" associated with seasonal variability in water quality, summer average values have been calculated for the primary factors thought to influence conditions in the lake (Table 4.1). Moreover, the summer represents the primary recreational season for the lake when boaters, skiers and others would be most aware of water quality conditions in the lake.

Table 4.1. Summer-average water quality conditions in Lake Elsinore: 2000-2009.

Summer	Z_{max} (m)	Total P (mg L^{-1})	Total N (mg L^{-1})	Avg TN:TP	Avg Chl (μg L^{-1})	TDS (mg L^{-1})
2000	7.4	0.11	2.56	24.1	48	1189
2001	6.5	0.11	3.72	34.8	111	1481
2002	4.9	0.16	4.71	32.1	255	2095
2003	5.4	0.47	5.87	13.4	182	1393
2004	5.8	0.42	7.19	16.2	197	1791
2005	10.5	0.56	2.40	4.3	52	1065
2006	9.2	0.40	2.43	6.7	78	1154
2007	7.8	0.19	4.01	24.1	56	1423
2008	7.4	0.15	1.99	13.9	24	1531
2009	6.9	0.15	4.01	26.7	87	1769

A simple correlation analysis was conducted to explore statistical relationships between summer-average chlorophyll a concentrations and total P, total N, TN:TP ratio, TDS and Z_{max} (Table 4.2). Summer-average chlorophyll a concentrations were most strongly correlated with total N (r=0.79) and TDS (r=0.70) and inversely correlated with

Z_{max} (r=-0.76). Summer chlorophyll a levels were not strongly correlated with total P or total N:total P ratio. Total N was positively correlated with TDS, reflecting similar concentration trends over time (Figs. 4.3 and 4.5, respectively) that indicate that total N behaves somewhat conservatively in the lake. Total P was inversely correlated with TDS, however, reflecting non-conservative behavior within the lake.

Table 4.2. Correlation matrix for measured water quality conditions in Lake Elsinore: 2000-2009.

	Chl a	**Z_{max}**	**TP**	**TN**	**TN:TP**	**TDS**
Chl a	1.00					
Z_{max}	-0.76	1.00				
TP	0.15	0.36	1.00			
TN	0.79	-0.71	0.24	1.00		
TN:TP	0.31	-0.63	-0.81	0.21	1.00	
TDS	0.70	-0.78	-0.39	0.57	0.60	1.00

Total N, TDS and Z_{max} were all statistically significant at p=0.01-0.03 and individually accounted for 49-62% of the variance in observed chlorophyll a concentrations (Table 4.3). Multiple linear regressions were also performed to quantify co-dependencies of chlorophyll a concentrations with nutrients, TDS and related water quality variables. TDS in combination with total N or total P in a two-variable regression model increased the r^2 values for the regression to 0.72 and 0.69, respectively. Incorporation of an additional 1-3 variables further increased r^2 values, reaching 0.92 when TN, TP, TDS, TN:TP and Z_{max} were included in the regression model, although the significance level varied somewhat due to the large number of fitting parameters. The multiple linear regression models that yielded the largest r^2-values are provided in equations (4.1)-(4.5).

$$Chl\ a = 26.96*TN + 0.085*TDS - 124 \quad (4.1)$$

$$Chl\ a = 221.5*TP + 0.211*TDS - 265 \quad (4.2)$$

$$Chl\ a = 18.3*TN + 123.3*TP + 0.136*TDS - 199 \quad (4.3)$$

$$Chl\ a = 5.79*TN + 388.0*TP + 4.75*TN{:}TP + 0.136*TDS - 315 \quad (4.4)$$

$$Chl\ a = -18.93*TN + 556.8*TP + 5.09*TN{:}TP + 0.099*TDS - 33.2*Z_{max} + 22 \quad (4.5)$$

Table 4.3. Results from linear and multiple-linear regression analyses predicting summer chlorophyll a concentrations in Lake Elsinore using 2000-2009 data.		
1-Variable Linear Regressions	**r^2**	**Significance**
Z_{max}	0.58	0.01
TP	0.02	ns
TN	0.62	0.01
TN:TP	0.10	ns
TDS	0.49	0.03
2-Variable Linear Regressions		
TP + TN	0.63	0.03
TP + TDS	0.69	0.02
TP + TN:TP	0.57	0.05
TN + TDS	0.72	0.01
TDS + TN:TP	0.50	0.09
TDS + Z_{max}	0.60	0.04
3+ Variable Linear Regressions		
TN+TP+TDS	0.76	0.03
TN+TP+TDS+TN:TP	0.83	0.04
TN+TP+TDS+TN:TP+Z_{max}	0.92	0.03

This simple statistical analysis indicates that total P alone is a poor predictor of summer-average chlorophyll a concentrations in the lake, while lake level, salinity and total N each individually account for 49-62% of the variance in observed chlorophyll a levels. Adding a 2nd variable predictably improved regressions, with TDS in combination with total P or total N accounting for 69-72% of the variance in chlorophyll a concentrations (Table 4.3). Incremental improvements were achieved by including remaining variables in regression models. At the same time, it is recognized that substantial autocorrelation exists in the data set, so care is needed to avoid over-interpretation of these findings. Moreover, this statistical analysis does not include changes in aquatic ecology, habitat and other factors in the lake, except indirectly through changes in lake level (Z_{max}) and TDS.

5. Summary and Conclusions

A wide range of sediment properties were evaluated, including the concentrations of organic C , $CaCO_3$, total N, total P, inorganic and organic P, and porewater NH_4-N and PO_4-P concentrations. Grouping the different sediments into the 3 types proposed in Anderson (2001) yielded no statistically significant differences for properties except for increased $CaCO_3$ in the fine organic (type III) sediments in 2010 relative to concentrations measured in 2000. Non-parametric statistical tests over the entire dataset (i.e., without prior assumptions about clustering of data) indicated that the sediments in 2010 had a slightly higher sand content, and increased porewater PO_4-P concentrations, but somewhat lower organic C concentration, loss-on-ignition, and porewater NH_4-N. Overall, current sediment properties do not provide clear evidence of changes in sediment quality over the past decade. That is, recycled water additions and related management actions have not substantively improved nor degraded sediment quality based upon these measurements.

Nutrient flux and sediment oxygen demand (SOD) rates were measured at 3 sites, representing the type I, II and III sediments, in August for direct comparison with measurements made in August 2001 (Anderson, 2001). The mean flux of PO_4-P from the fine organic type III sediment at low native DO concentrations (0.5 mg L^{-1}) increased from 10.1±0.3 in 2001 to 12.8±1.2 mg m^{-2} d^{-1} in 2010, while flux from the type II sediment decreased from 10.5±0.9 to 7.8±3.1 mg m^{-2} d^{-1}. The coarse-textured type I sediment was found to release PO_4-P at a slow rate in 2001 (1.9±0.9 mg m^{-2} d^{-1}), while it took up PO_4-P at a slow rate (-1.1±0.2 mg m^{-2} d^{-1}) from the water column in 2010. Mean NH_4-N flux was somewhat higher in 2010 in the type I and III sediments and unchanged in the type II sediments. Aeration was found to reduce PO_4-P flux by 29% in the fine organic type III sediments, but had less of an effect on the other sediments. Average NH_4-N flux rates were not significantly altered as a result of aeration.

Additional measurements provided new information about sediment biogeochemistry. *In situ* measurements of gas volume found negligible volumes in March, but very high volumes within the sediments in July and August. The volumes of gas within sediments in the summer were generally 1-2 L m^{-2} at most sites, with a maximum measured volume of almost 6 L m^{-2} in a silt-rich sediment near the mouth of the channel leading to the San Jacinto River input to the lake. The gas there was elevated in CO_2 over 100x that found in air (3.8±0.6% CO_2 by volume, compared with

approximately 0.035% in air), reflecting rapid rates of microbial respiration and decomposition in the warm summer sediments. No significant O_2 was measured in the gas samples, with most of the remaining gas as N_2.

Microprofile measurements of pH and redox indicate limited penetration of DO into the sediment under vigorous aeration; aeration at a rate that is estimated to be over 1000x more rapid that the lake-wide average aeration rate achieved DO penetration 3-4 mm after 1 week. This clearly reflects the intense microbial activity occurring near the surface of the sediments. Sequential extraction of surface sediments demonstrate significant quantities of reactive iron-sulfide minerals present, with FeS(am) and Fe_3S_4 in sufficient quantities to exert a significant demand for oxygen. The quantities of extractable reduced Fe(II)-sulfide and oxidized Fe(III) minerals exhibited no significant difference in a transect between two adjacent diffuser lines, implying the diffused aeration system has not been able to favorably alter sediment biogeochemical conditions there. Observations about sediment color support this conclusion.

In addition to these direct, detailed sedimentological measurements, multi-frequency hydroacoustics were used to determine depth to sediments and sediment acoustical properties. Surveys on transects totaling 270 km in length were conducted over 6 days in late June and early July. All hydroacoustic data were georeferenced using realtime differential GPS that allowed development of detailed bathymetric maps and maps of acoustically-inferred sediment properties based upon the strong correlation between the fractal dimension of the bottom echo and organic C content, % water content and other sediment properties.

Finally, water quality data from 2000-2009 were reviewed and statistically analyzed. The mean summer chlorophyll a concentrations over the past 10 years were found to be significantly correlated with maximum depth, and concentrations of total N and TDS (r^2 = 0.58, 0.62 and 0.49, respectively, but not correlated with total P or total N: total P ratios (r^2 = 0.02 and 0.10, respectively). Lake level and TDS thus appear to be more important predictors of summer chlorophyll a concentrations that total P concentrations in the lake.

6. References

Anderson, M.A. 2001. *Internal Loading and Nutrient Cycling in Lake Elsinore.* Final Report. Santa Ana Regional Water Quality Control Board. 52 pp.

APHA 1998. *Standard Methods for the Examination of Water and Wastewater.* 20th Edition. American Public Health Association, Washington, D.C.

Aspila, K.I., H. Agemian & A.S.Y. Chau, 1976. A semi-automated method for determination of inorganic, organic and total phosphate in sediments. Analyst 101: 187-197.

Berner, R.A., and J.L. Rao. 1994. Phosphorus in sediments of the Amazon River and estuary: implications for the global flux of phosphorus to the sea. Geochim. Cosmochim. Acta 58:2333-2339.

de Koff J, Anderson MA, Amrhein C. 2008. Geochemistry of iron in the Salton Sea, California. *Hydrobiol.* 604:111-121.

Elci, S, A. Bor and A. Caliskan. 2009. Using numerical models and acoustic methods to predict reservoir sedimentation. *Lake Reserv. Manage.* 25:297-306.

Gee, G.W. & J.W. Bauder, 1986. Particle-size analysis. In Klute, A. (ed.) Methods of Soil Analysis. Part 1. 2nd ed. Agronomy Monographs 9. ASA and SSSA, Madison, WI: 383-411.

Hakanson, L. & M. Jansson. 1983. Principles of Lake Sedimentology. Springer-Verlag, New York, NY.

Loeppert, R.H. & D.L. Suarez, 1996. Carbonate and gypsum. In Sparks, D.L. (ed.) Methods of Soil Analysis. Part 3. 3rd ed. Agronomy Monographs 9. ASA and SSSA. Madison, WI: 437-474.

Lord C.J., III, 1982. A selective and precise method for pyrite determination in sedimentary materials. Journal of Sedimentary Petrology 52: 664-666.

Nelson, D.W., and L.E. Sommers. 1982. Total carbon, organic carbon, and organic matter. In Page, A.L., R.H. Miller & D.R. Keeney (ed.) Methods of Soil Analysis, Part 2. 2nd ed. Agronomy Monographs 9. ASA and SSSA., Madison, WI: 539-580.

Ostrovsky, I., D.F. McGinnis, L. Lapidus and W. Eckert. 2008. Quantifying gas ebullition with echosounder: the role of methane transport by bubbles in a medium-sized lake. Limnol. Oceanogr. Meth. 6:105-118.

Raiswell R. & R.A. Berner, 1985. Pyrite formation in euxinic and semi-euxinic sediments. American Journal of Science 285: 710-724.

Rowan, D.J., J. Kalff & J.B. Rasmussen, 1992b. Profundal sediment organic content and physical character do not reflect lake trophic status, but rather reflect inorganic sedimentation and exposure. Canadian Journal of Fisheries and Aquatic Sciences 49: 1431-1438.

Wetzel, R.G. 2001. Limnology: Lake and River Ecoystems. 3rd ed. Academic Press, San Diego, CA. 1006 pp.